ACE Deliverable 2.1-D4

Report on facilities benchmarks

Project Number: FP6-IST 508009

Project Title: Antenna Centre of Excellence

Document Type: Deliverable

Document Number: FP6-IST 508009/ 2.1-D4

Contractual Date of Delivery: 31 December 2005

Actual Date of Delivery: 6 January 2006 (with cover-page + reviews)

Workpackage: Mainly WP 2.1-3, but also related to WP 2.1-1 & 2.1-2

Estimated Person Months: 8

Security (PU,PP,RE,CO): PU

Nature: R (Deliverable Report)

Version: rev 0 for the main document

Total Number of Pages: 80

File name: ACE_2.1D4_total.pdf

Editors: Hervé Legay, Peter Gardner, Olivier Lafond

Other Participants: Oliver Vendier, Juha Ala-Laurinaho, Mohamed Himdi, Ronan Sauleau, Carlos Fernandes + all institution members of WP2.1.3 for inventory (table-appendix B)

Abstract

This report includes some benchmarking tests on challenging designs and technologies that were identified in the former Deliverable (2.1-D3).

Keyword List

integrated antennas, millimetre-wave antennas, precision etching, reflectarray, Micromachining, MEMS, lenses,

1 INTRODUCTION

This report aims at benchmarking challenging designs and technologies that were identified in Deliverable 2.1-D3.

Many technologies are involved in the manufacturing of integrated antennas, which are very different from those used in conventional antennas. They were reviewed in deliverable 2.1-D3 :

- Active integrated antennas, an issue is the accommodation of active devices within the radiating element, in order to improve its compactness or to add new functionalities. All technologies related to semiconductor and packaging are therefore concerned ;
- For millimetre wave and sub millimetre wave integrated antennas, high accuracy is required for the antenna parameters. Micromachining technologies are therefore of special interests ;
- Structural materials such as substrates, multilayer circuits, dielectrics are also used for the radiating element, with special specifications according to the applications ;
- Micromachined electro-mechanical systems (MEMS) also offer huge opportunities for novel high performance antennas ;

A number of potential applications have been reviewed, which illustrate the potential improvement brought by the detailed technology.

The objective of this document is to select some of these challenging applications, and to identify for each one some critical issues, related to these technologies. It could be related to the reliability of the process, to the accuracy, to its limit in terms of frequency band, etc..

The selected applications are :

- Reconfigurable Reflectarray with MEMS ;
- Printed Antenna Array at 60 GHz with a multilayer technology and a thick ground plane ;
- Air spaced mm-wave patch antennas fabricated using Electric Discharge Matching (EDM) ;
- Lens antenna for a shaped coverage ;
- Dielectric Rod Waveguide antenna for 170 GHz ;

European Commission - 6th Framework Programme	ACE (Antenna Centre of Excellence)	Information Society Technologies

Reconfigurable Reflectarray with MEMS Switches

Institution	Authors
Alcatel Alenia Space	Hervé LEGAY

Document Evolution		
Revision	Date	Reason of change
0	28-11-05	

1. OBJECTIVES

MEMS (Microelectromechanical Systems) technology plays a key role in the on-going miniaturization of electronic modules and systems in future telecommunications systems, but also automotive and consumer electronics subsystems. While MEMS operating in the low-frequency region are currently being employed e. g. as acceleration sensors in automotive applications, the field of RF (radio frequency) MEMS is still in a state of research and early development mainly in US and Asia (Radant, Magfusion, OMRON, Hitachi…). RF MEMS switches exhibit excellent RF properties as low power consumption, high linearity, low loss and high isolation. In addition, MEMS can very straightforwardly be integrated into RF subsystems to achieve a higher degree of functionality, for example in active antenna.

On the other hand, antennas are probably the best area for the application of this new technology. It is particularly believed that MEMS technology may open solutions for cost-effective satellite antennas that provide reconfigurable coverage. This feature is for instance more and more requested for instance by telecommunication operator with the goal to offer flexible broadcast services according to the market demand evolution. And there is currently no technical solution at moderate cost.

Thanks to the miniaturization of electronic modules provided by MEMS technology, it becomes now possible to integrate MEMS switches within the radiating elements, and to merge electronic and radiating functions. Such MEMS based antennas will then be processed at large scale with an industrial process defined to reach very low manufacturing costs. This also results in lightweight, low consumption and low volume, and consequently in a dramatic breakthrough for a reconfigurable antenna.

MEMS based elements for reflectarray elements have been designed by Alcatel Alenia Space in collaboration with IETR. The objective is now to manufacture the reflectarray elements with MEMS switches, and to identify the key technological issues.

This case has been initiated by Alcatel Alenia Space in collaboration with LAAS and Thales Research and Technology, under an ESA contract. A first run has been manufactured and tested. The benchmarking test will be extended to AMICOM partners contributing to a Reflectarray project called RARPA.

2. DESIGN OF THE PHASE SHIFTER ELEMENT

2.1 SPECIFICATIONS

The following stringent requirements were selected for the design of the phase shift element :

- low loss, lower than 0.5 dB
- phase quantisation better than 3 bits,
- large bandwidth (7% in Ku band),
- 0.6 λ array lattice,
- low cross-polarisation,
- low cost for industrial manufacturing,
- robustness with respect to the manufacturing tolerances

The following frequency bands were selected :

- For the telecommunication applications, the application which benefits the most from reconfigurability is DBS TV. The band is 11.7-12.5 GHz, which gives a 6.6 % relative bandwidth ;
- For data transmission, the allocated band is set to 50 MHz, which can be allocated anywhere within a 500 MHz range (26.15 – 26.65 GHz).

2.2 PRINCIPLE OF OPERATION OF THE PHASE SHIFTER ELEMENT

The design of the active phase shift element is an extension of the work carried out by IETR and Alcatel Alenia Space on passive phase shifter elements [1]

The designed concept consisted of a slotted patch element. It was demonstrated that by changing simultaneously the patch and the slot length, is was possible to achieve a phase shift range greater than 360°, and to have smooth variation of the phase shift with frequency. The main interest of this phase shift element is that it combines simultaneously a low Q factor, i.e. a large frequency bandwidth, and manufacturing simplicity, since only one layer is required.

[1] "New reflectarray cell using coupled microstrip patches loaded with slots", D. Cadoret, A. Laisne, R. Gillard, H. Legay, Microwave and Optical Technology Letters, Vol. 44, N°3, Feb. 2005, pp. 270-273

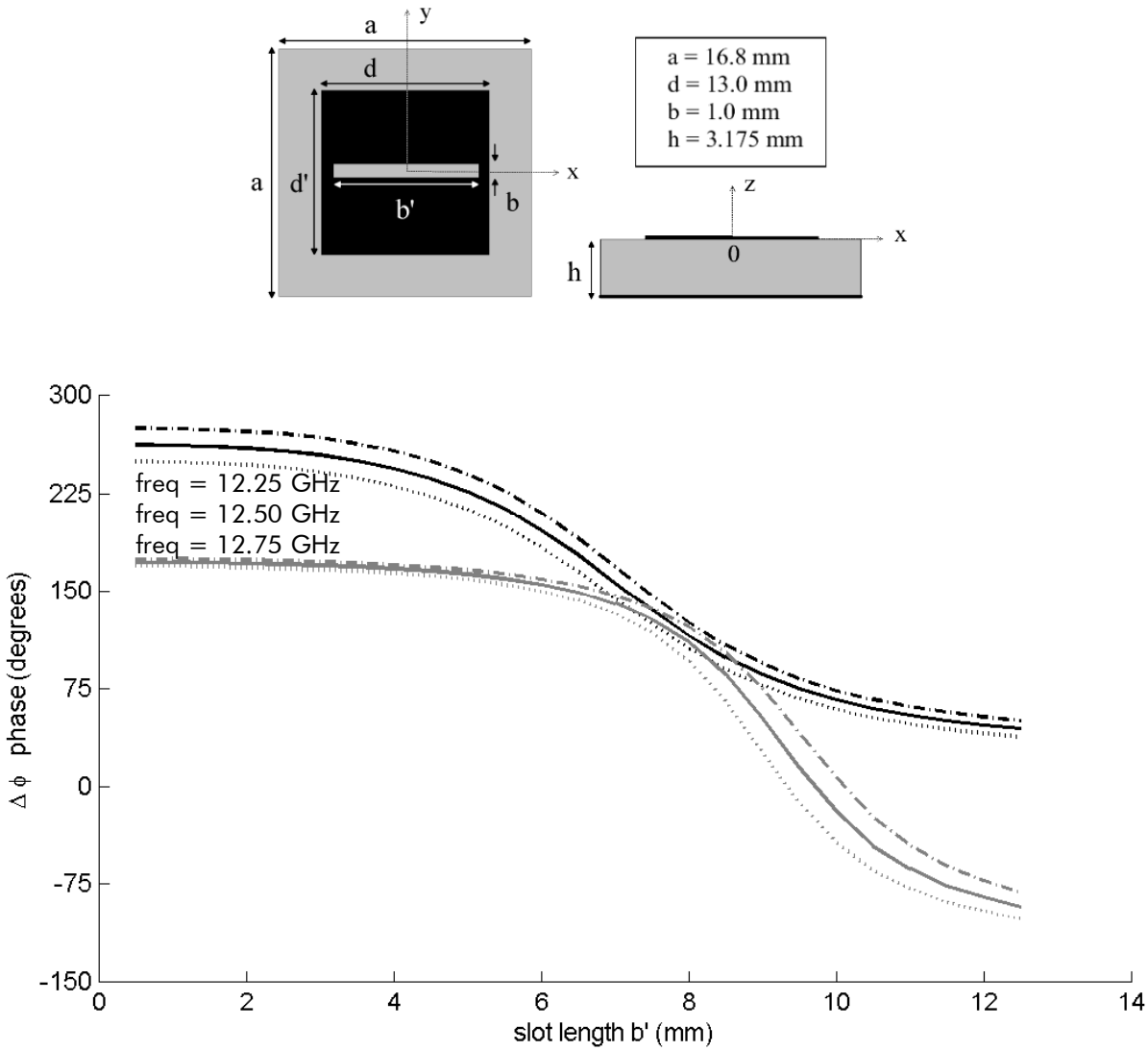

Figure 2.2-1 : Concept of a phase shift element based on a patch loaded with a slot. Corresponding Phase variations versus slot length for two patch length, at 12.25, 12.5, 12.75 GHz.

We then devised the extension of this concept for active phase shift elements, with MEMS control. We came up to the design of a phase shift element, which consists in three patch sections separated with 0.5 mm gaps, as presented in Figure 2. These patch sections can be interconnected to each other by MEMS switches, distributed along the gaps.

When the MEMS located in the edges of a gap are in down position, the gap is then converted into a slot.

Depending on the MEMS up and down positions, the active length of the slot varies, as shown in the following figure. It is then possible to have a phase shift element, which can consist of a patch section, a long patch with two slots, a shorter patch with one slot closed to a patch section, etc.

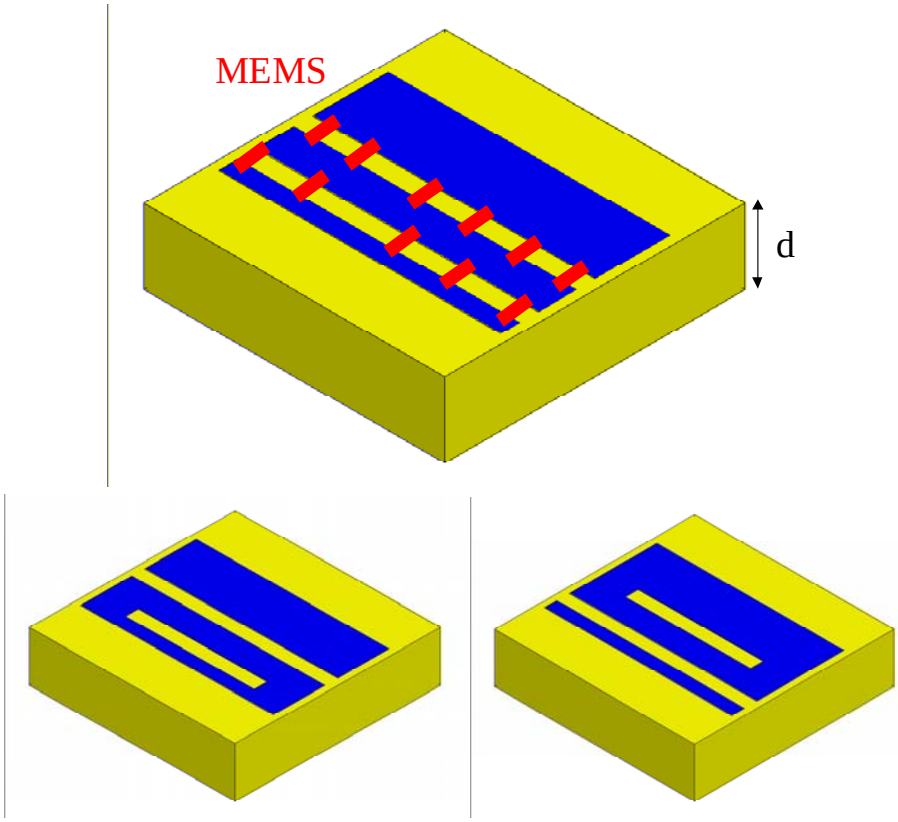

Figure 2.2-2 : Active Phase shift element with MEMS switches. Example of equivalent phase shift elements which can be obtained.

2.3 TYPICAL PERFORMANCES

The optimisation of the phase shifter element was first carried out with HFSS . The phase shifter element was simulated assuming an incident plane wave on an infinite array of similar elements. Periodic boundary conditions were then used for HFSS.

As shown in Figure 2.3-2, the results indicates that the full range 0-360° is achievable with a passive slotted element equipped of two slots of variable length. A desired phase shift can be achieved with a number of combinations of the length of the two slots, demonstrating the intrinsic redundancy capabilities of the design.

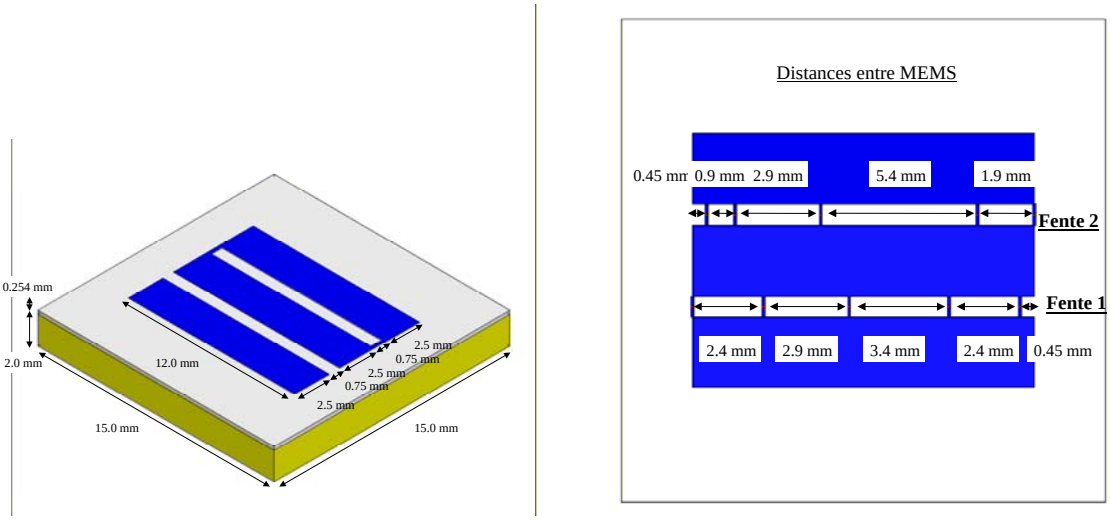

Figure 2.3-1 : achieved design in Ku band

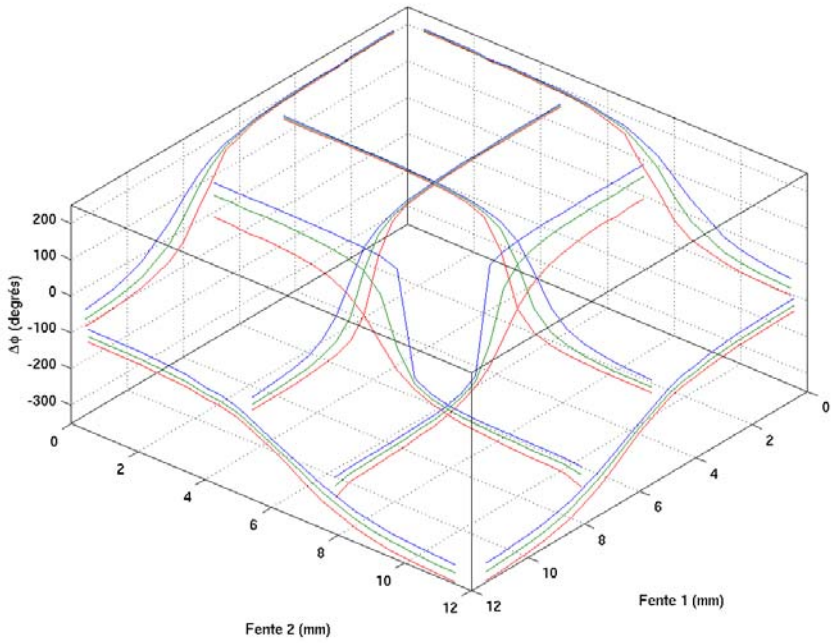

Figure 2.3-2 : Variation of the equivalent passive phase shift element (in ordinate) with the variation of the two slot lengths (in abscissas). No MEMS is considered here. Blue :11.7 GHz, Green : 12.1 GHz, Red : 12.5 GHz

Once the parameter of the phase shift element were set, the phase shift element was simulated with MEMS switches. 5 MEMS were distributed over each slot. For the first iteration, pure short and open circuits were considered for the load when the MEMS is in down or in up position.

Specific cases were simulated. Comparison with the passive phase shift element was performed, assuming the slot length equal to the maximum distance between MEMS in down position. The discrete points showed a satisfactory comparison between the equivalent passive element and the active element with MEMS switches.

It has to be mentioned that due to the diversity of scale, and to the requested meshing in HFSS, simulation were altered by convergence problems.

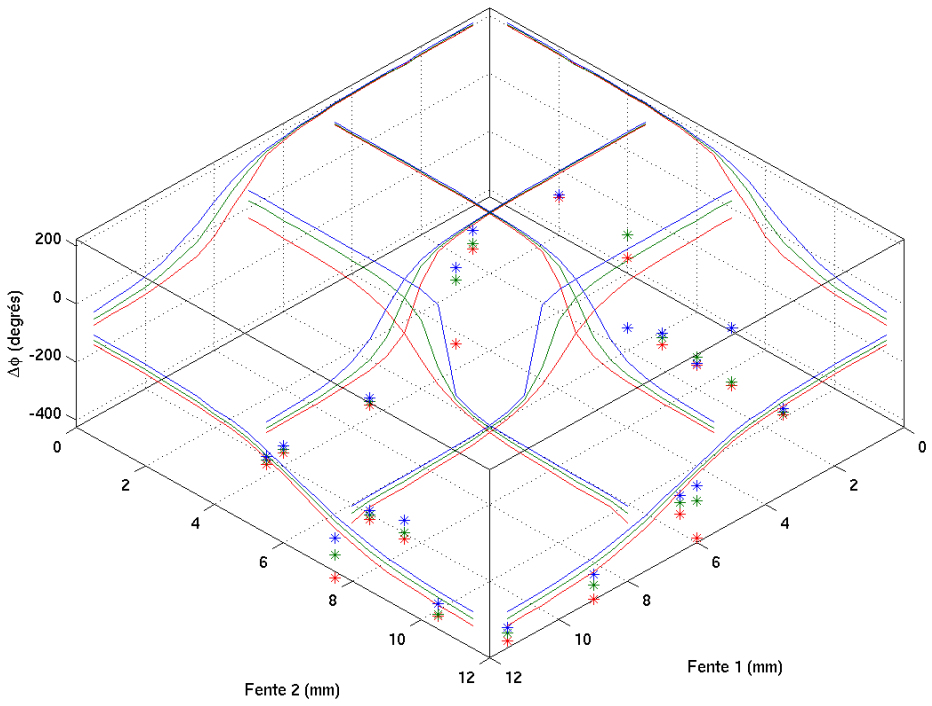

Figure 2.3-3 : Comparison of phase shift with MEMS with the equivalent passive phase shift element. The equivalent slot length is equal to the distance between MEMS switches. Blue :11.7 GHz, Green : 12.1 GHz, Red : 12.5 GHz

A specific electromagnetic modelling tool was then developed by ENSEEIHT[2], which could manage the high diversity of scales within the antenna (the phase shift element, the MEMS circuits). The proposed model offers a substantial reduction in computer time and memory over many direct full-wave methods. The tool has been successively benchmarked with HFSS. The computation of all phase shift states can be computed quasi immediately with a post processing varying successively the impedance of the MEMS.

Scanning these 1024 states corresponding to the combination of the Up or Down Positions fot the 1024 MEMS switches has then been down. It demonstrated that a very regular phase distribution in the 0-360° range can be achieved, The average phase quantization step is very low. Dots in blue correspond to configurations which have been crossed checked with HFSS.

[2] "N-port Network for the Electromagnetic Modeling of MEMS Switches," E.Perret, H.Aubert, R. Plana, Microwave and Optical Technology Letters, April 5, 2005

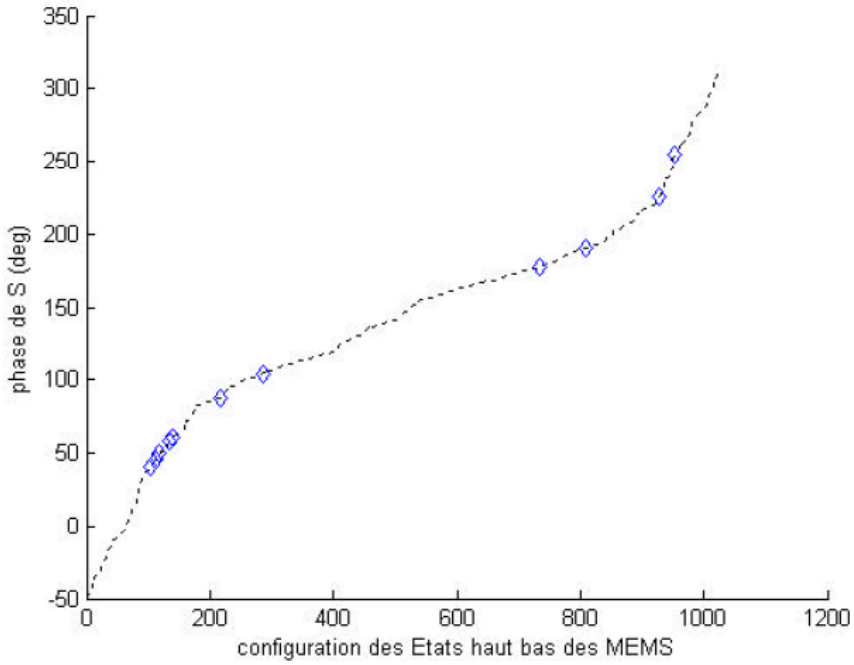

Figure 2.3-4 : Distribution of the 1024 Phase shift states

2.4 TOPOLOGY OF THE ELEMENT

2.4.1 Multilayer Assembly

The parametric study carried out on the concept presented in the previous sections indicated that the slotted patch element should be separated from the ground plane by a material which has the smallest effective permittivity.

A suspended approach is then selected, consisting in a thin layer of a substrate on which patches and MEMS made, suspended on an air spacer layer. This approach permits to keep the effective permittivity for the phase shift element as close as possible to the permittivity of the air.

The antenna is made by mounting Wafers of the selected material (either micromachined Silicon or Alumina) on a support plate, the function of which is to :

- Achieve the cavities which are requested in the design, and which permit to reduce the coupling between neighbouring phase shift elements ;
- Interconnect the silicon module and multilevel DC supply board in order to bias the MEMS ;

Solutions which permits to cope with thermal mismatch between the materials are identified. The use of an array of metallized plastics with CIN : APSE interconnectors is one of them.

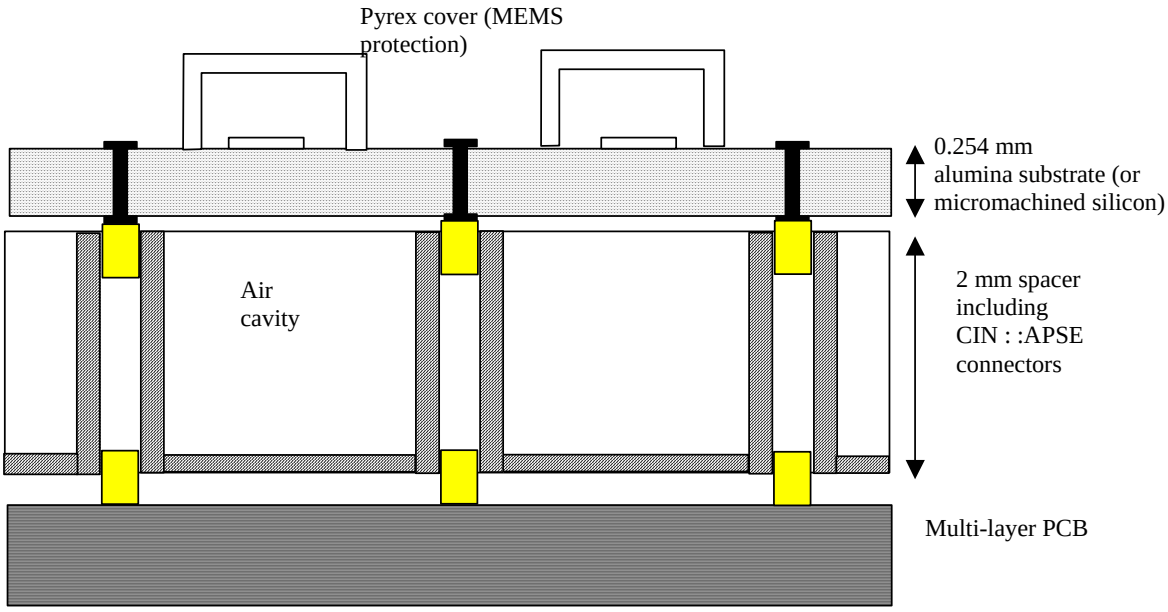

Figure 2.4-1 : *Concept for Antenna interconnection with control circuitry (not on scale*)

2.4.2 Choice of the materials

Several materials were considered for the wafer plate. Their main electromagnetic characteristics are summarised in the table below.

		HR Si	**7740 Pyrex**	**7070 Pyrex**	**GaAs**	**Al_2O_3**
Resistivity (Ohm.cm)	25 °C	$2\ 10^{3}$ to 10^{3}	$2.\ 10^{11}$		10^{7}	$>10^{E14}$
Epsilon R	1 MHz	11.7	4.6	4.1	12.9	9.9
	100 GHz		4.5			
Tan delta	1 MHz		5.10^{-3}	6.10^{-4}	5.10^{-4}	1.10^{-4}
	100 GHz	$2\ 10^{-3}$ $2\ 10^{-4}$	$12.5\ 10^{-3}$		3.10^{-4}	3.10^{-4}
Thermal conductivity (W/m K)	25 °C	170	1.1		46-55	35

Table 2.4-1 : Electromagnetic Characteristics of main material of interest

The following constraints governed the choice of the materials:

- It shall indicate a low loss tangent in order to have low losses in the reflectarray elements,
- It shall be compatible with MEMS manufacturing,

- The proposed concept implies to connect the MEMS to its command circuitry through via holes in the substrate.

Isolated via holes are difficult to produce in some material (such as Silicon, Pyrex), and in any case, far from standard in micro-electronic processes.

In contrast, via holes in ceramic substrates are standard and require little tooling. However, Alumina presents higher electromagnetic characteristics in term of losses (lower tan δ), but has a high surface roughness.

The two selected materials were :

- Silicon, as it is a standard substrate for MEMS. It will be micromachined in order to have low loss.

- Alumina, for its low loss tangent. Due its poor roughness characteristics, the MEMS will be in a frozen stage (either in up or down position). Discussions with several potential alumina suppliers have led to the following general characteristics for the substrate : Thickness 254 µm, Polished surfaces

3. BENCHMARKING CASES

Two detailed designs were derived :

- In Ku band, for a GEO telecom mission with flexible coverage, pseudo-active phase-shift elements (MEMS frozen Up or Down) are manufactured by Thales R&T on alumina ;
- In Ka band, for high data rate transmission between satellites, active phase-shift elements on micro-machined silicon are built by LAAS ;

3.1 PHASE SHIFTER ELEMENT IN KU BAND

3.1.1 Technological choices

Alumina is chosen as the substrate used for the MEMS and the patch element. The main interest of this material is its low loss tangent. Another advantage is the availability of alumina substrates with filled via holes. These vias are required in a full scale demonstrator for routing the control signals to the MEM switches.

The technology demonstrator on alumina proved to be difficult to realise due to the combination of specific requirements not present before :

- Alumina substrate required surface aspect : for the MEMS process a very good surface finish is required, as can be found on regular silicon wafers (mirror finish) ;
- Substrate thickness: in order to meet the RF performances we chose the thinnest available alumina substrates. Even though 254 µm remains a standard thickness, the substrates are highly fragile and prone to breaking. Substrate fragility is considerably increased by the presence of 1000 via holes per plate.
- Hole pitch: metal bridge appears between two vias at the end of the electrolysis process used to fill the vias with metal; these bridges create stresses during the subsequent polishing process that leads to breakage of the substrate ;

As a first run, the decision was taken to have MEMS frozen in up or down states. This is a 5 mask levels process without packaging. The layout includes command lines and electrodes even though the switches are placed in fixed UP or DOWN configurations. This ensures the same electromagnetic behavior as for a fully active antenna pattern.

3.1.2 Description of the manufactured cells

The engineered cells are made of four different types. The first variation concerns the MEMS topology, having a type 1 MEMS perpendicular to the line or a type 2 MEMS parallel to the line, as shown in the figures below.

The two anchorages of the bridge are isolated from patch metallisation for DC to avoid DC short circuit. And only one anchorage is isolated from patch metallisation for RF. The RF short circuit and DC isolation of one anchorage is obtained by thin dielectric layer with high capacitance area.

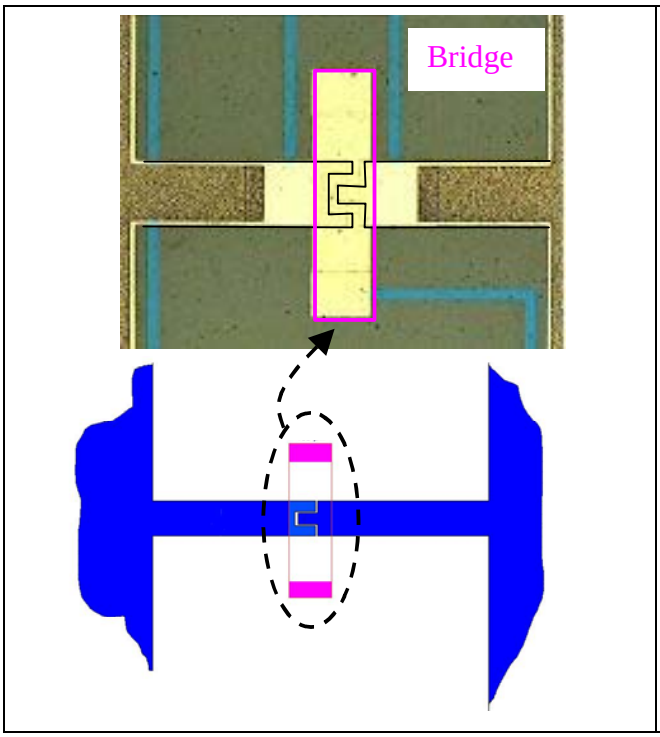

Figure 3.1-1Type 1 MEMS

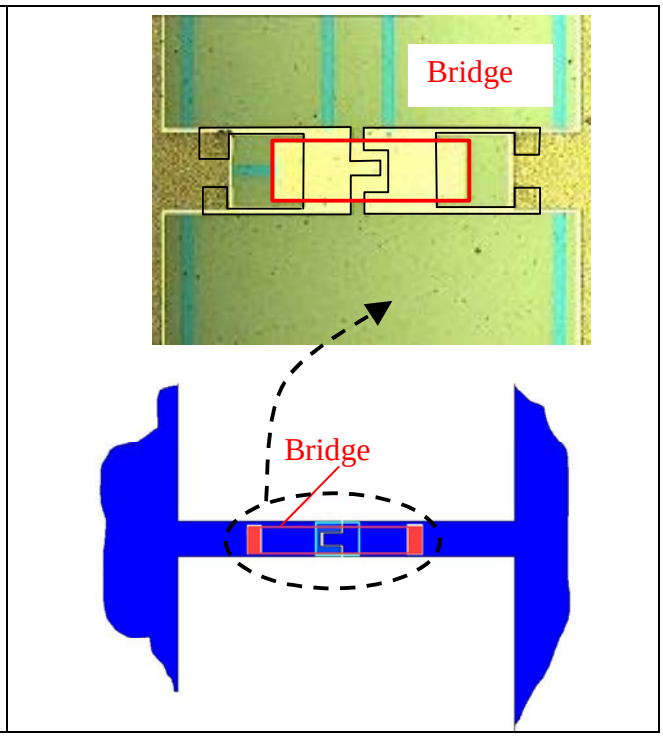

Figure 3.1-2Type 2 MEMS

The second difference is introduced by using two alumina substrates, one with via-holes and the other without via-holes. Some manufacturing problems with our Alumina suppliers , originally expected with via-holes, orientated us to supply with other alumina substrates, which were not equipped with via holes.

The via-holes are required to ensure the electric continuity from the square waveguide to the metallic cavity. Via-holes are made by laser drilling and filling of via-holes by electrolysis. Each cell includes sixty 200µm diameter via-holes with a 1 mm pitch.

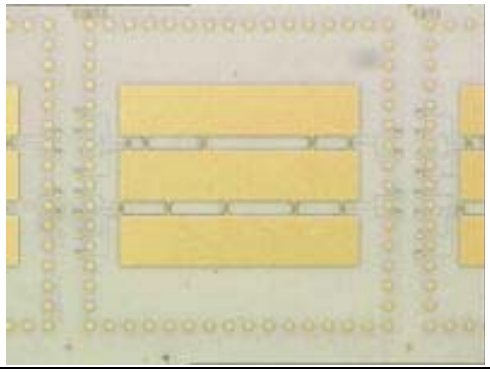

Figure 3.1-3 : RIE type MEMS, with via-hole

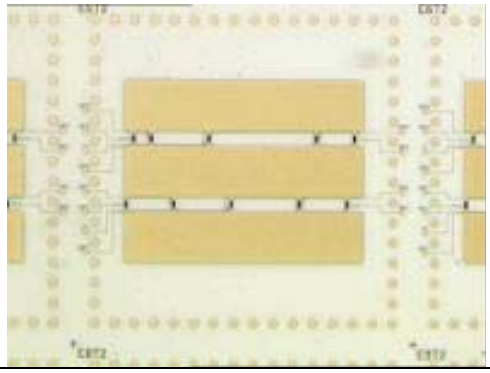

Figure 3.1-4: TRT type MEMS, without via-holes

3.2 PHASE SHIFTER ELEMENT IN KA BAND

3.2.1 Technological choices

This slotted patch is printed on a 400 µm silicon layer, which is micro-machined to reach a 50 µm thickness under the patch area. The micromachining is required for reducing losses.

Three wafers have been processed with the fabricated mask. But only one wafer has reached successfully the bridge fabrication step. As the final silicon etching step is very difficult we have chosen to suppress this step in order to be sure to obtain some samples. Then the components are not on dielectric membrane but on 50µm thick silicon membrane.

3.2.2 Description of the cells

The slotted patch has then to be etched on a very thin dielectric membrane. As the membrane surface was set to few square millimetres, a new membrane process was developed in order to obtain a more reliable membrane. The membrane is made with PECVD SiOxNy which allow up to 5µm thick layers, as compared to a 1.4 µm thickness with the previous process (based on SiO2/SiNx).

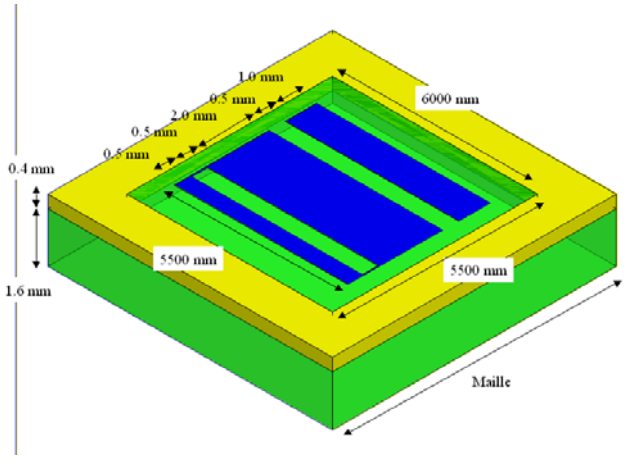

Figure 3.2-1 : Phase shift element in micromachined Silicon in Ka band

The new SiOxNy membrane was developed, and benchmarked with the SiO2/SiNx membrane for the case of a transmission line. The losses were measured very low and comparable for both membranes. This membrane could then be used for the phase shift element.

After the study of several potential design with microwave designer, we have chosen to fabricate antenna with 5 and 4 active MEMS for each slot. Several passive structures with MEMS on down position and without MEMS have been selected in order to evaluated the optimal characteristic and the parasitic effects. Switches have been also designed to evaluate the MEMS capacitance in the down position and mechanical tests structures have been implemented to control the technological parameter.

shows an example of active cell with 5 MEMS for each slot and with tests structures around the active part.

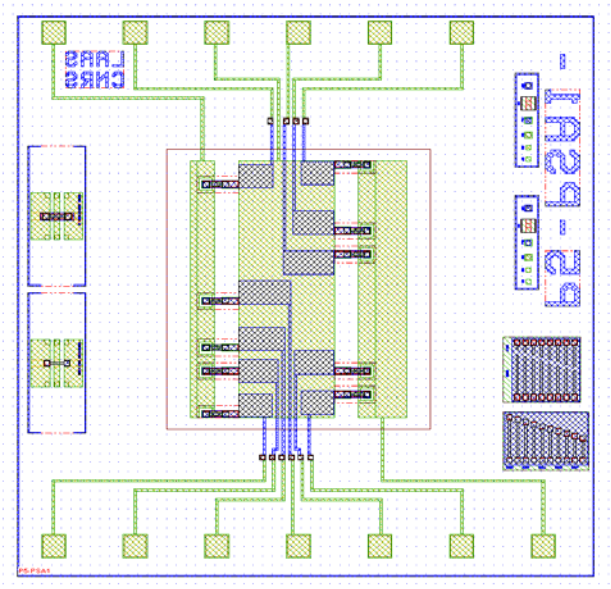

Figure 3.2-2 :Mask of a phase shift element in micromachined Silicon

The detail of the switch is presented below.

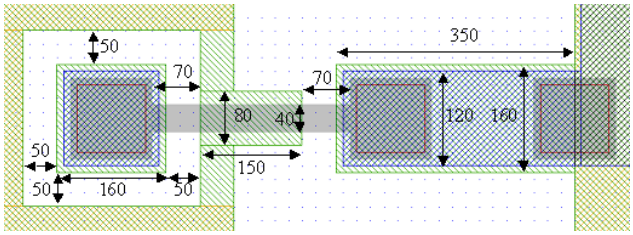

Figure 3.2-3 :Topology of the MEMS Switch

The MEMS is perpendicular to the slot. The two anchorages of the bridge are isolated from patch metallization for DC to avoid DC short circuit. And only one anchorage is isolated from patch metallization for RF. The RF short circuit and DC isolation of one anchorage is obtained by thin dielectric layer with high capacitance area.

Cells without MEMS are made to provide a reference case (Figure 3.2-4). Cells with MEMS are in a fixed up or down state (Figure 3.2-5) are also manufactured. Among the different available states, some regularly distributed phase-shift configurations were chosen to be engineered and their phase-shift measured. Active cells (Figure 3.2-6) include MEMS that can be turned in up or down position. This kind of cell is engineered with polarisation lines, comparison with passive cells will permit to observe the polarisation lines effect. The active cells are made with 4 to MEMS per slot.

Tests structures around the active part can be seen on the displayed Figure 3.2-7, they have been implemented to assess the MEMS capacitance in the down and up position and also mechanical tests structures have been implemented to control the technological parameters.

Detailed views of a realised cell is shown in Figure 3.2-7.

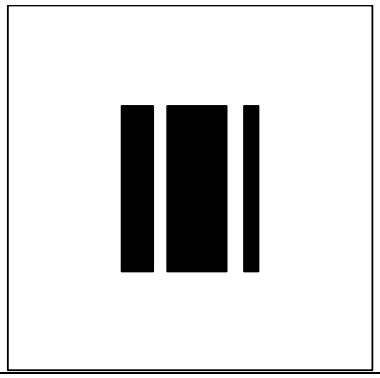

Figure 3.2-4: Cell without MEMS

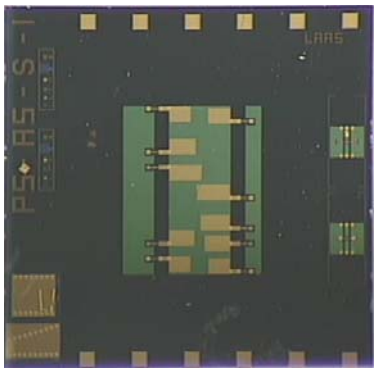

Figure 3.2-5: Semi-active cells, with fixed state MEMS

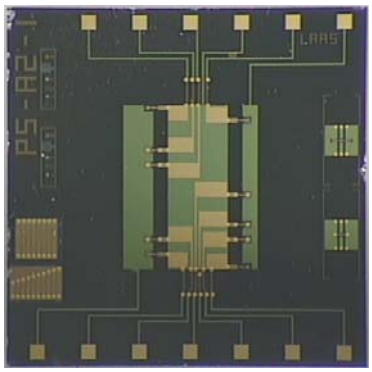

Figure 3.2-6: Active cells, with commandable MEMS

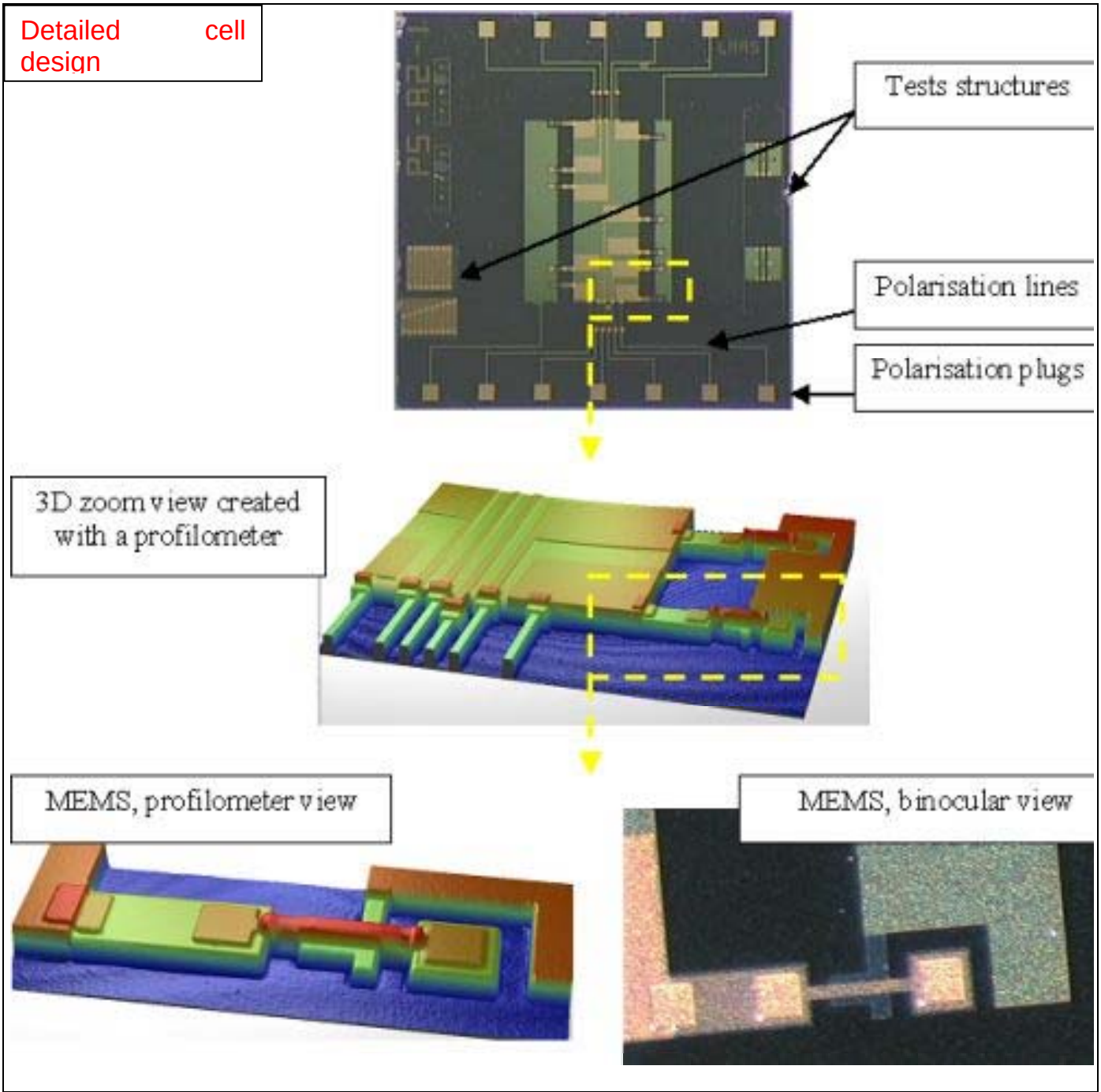

Figure 3.2-7: Description of a manufactured cell

4. TESTS DEVICES

The phase shifter elements are tested in a waveguide device. The test device in Ku band permits to test only passive phase shifter elements. The test device in Ka band permits to test controllable phase shifter elements.

4.1 TEST-DEVICE IN KU BAND

The test device includes a standard WR75 waveguide (operating from 10 to 15 GHz), a standard to square waveguide transition with a smooth transition , and a metallic cavity where the alumina module can be accommodated.

The substrate used to process a reflectarray element with MEMS is inserted in the cavity. It is hold by notches in the cavity. Via-holes in the substrate are required to ensure the electric continuity from the square waveguide to the metallic cavity as described in Figure 4.1-2.

The distance which separates the bottom of the cavity from the substrate is equal to the thickness of the spacer layer in the element design. The bottom of the cavity acts as a ground plane. This enables to assess directly the effect of the substrate without having to glue it to a spacer layer.

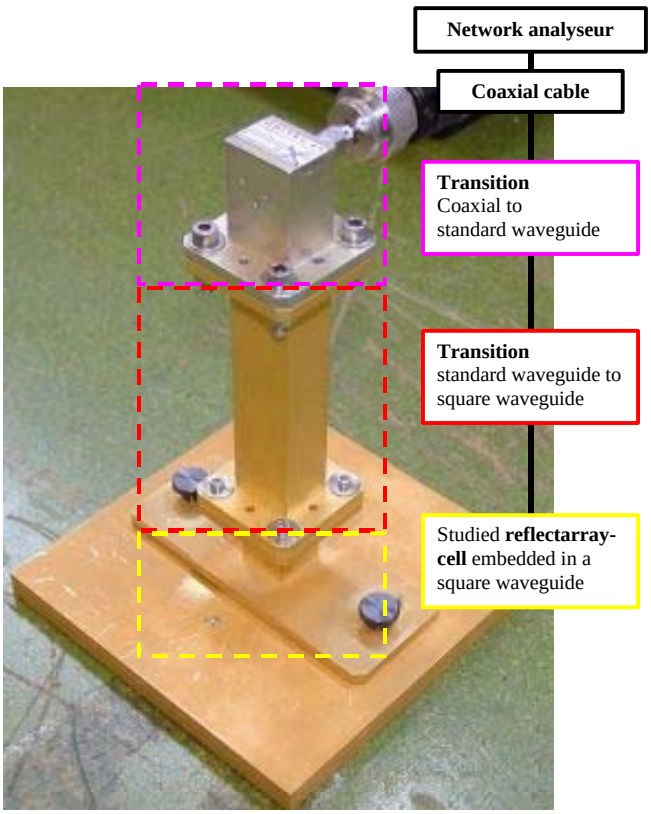

Figure 4.1-1 : Test device design in Ku band

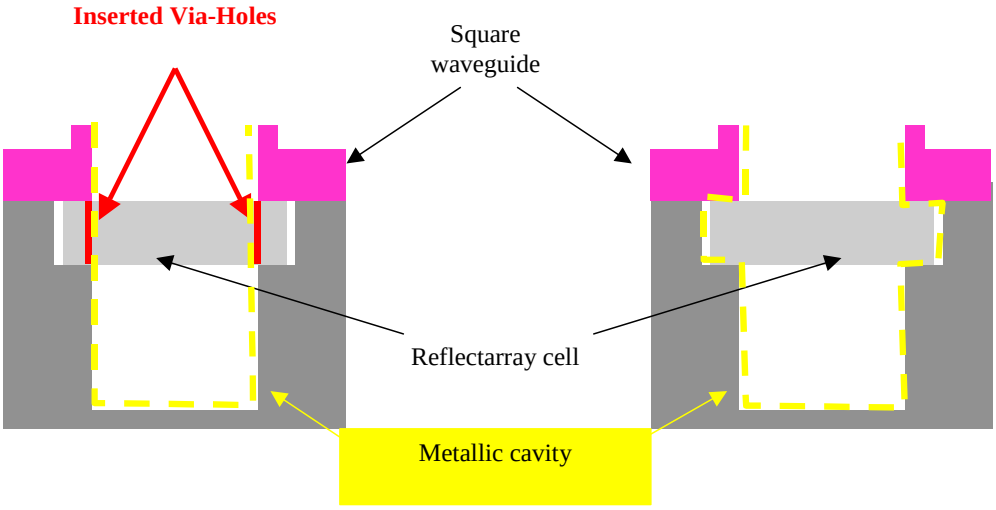

Figure 4.1-2 : Description of the via-holes impact.

This test device was first benchmarked, making sure that two measures give the same results.

4.2 TEST DEVICE IN KA BAND

The test device includes a standard WR34 waveguide (operating from 20 to 33 GHz), a standard to square waveguide transition with a smooth transition, and a metallic cavity where the silicon module can be accommodated. It also includes a control board which drives the biasing of the active MEMS. Needle-shaped connectors are used which are connect to electrodes on the active cells.

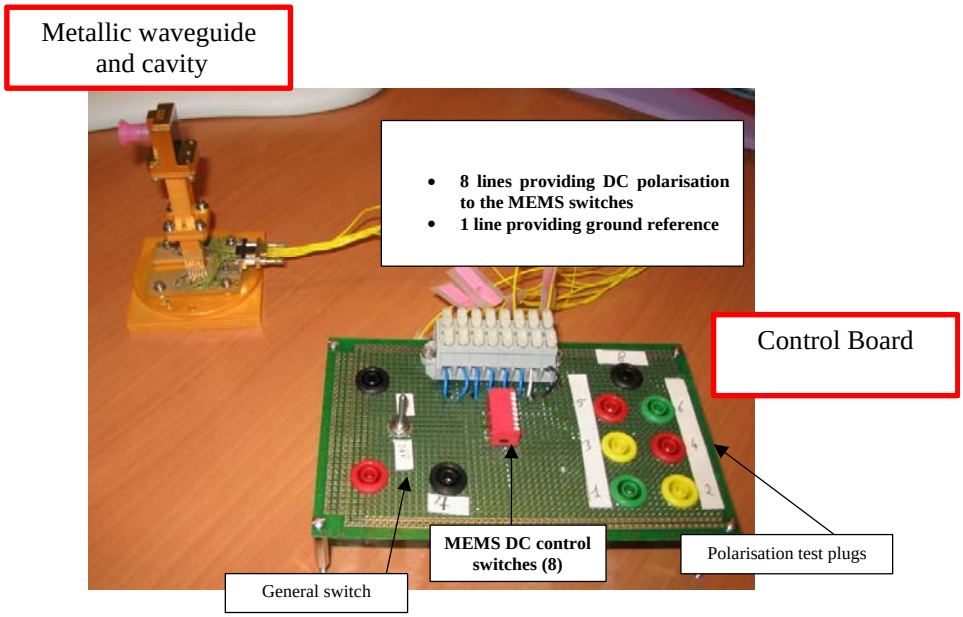

Figure 4.2-1 : *Test device for MEMS based cells*

The following figure shows the disposition of the MEMS in the reflectarray cell and the alignment between needle-shaped connectors and polarisations plugs included onto the cell.

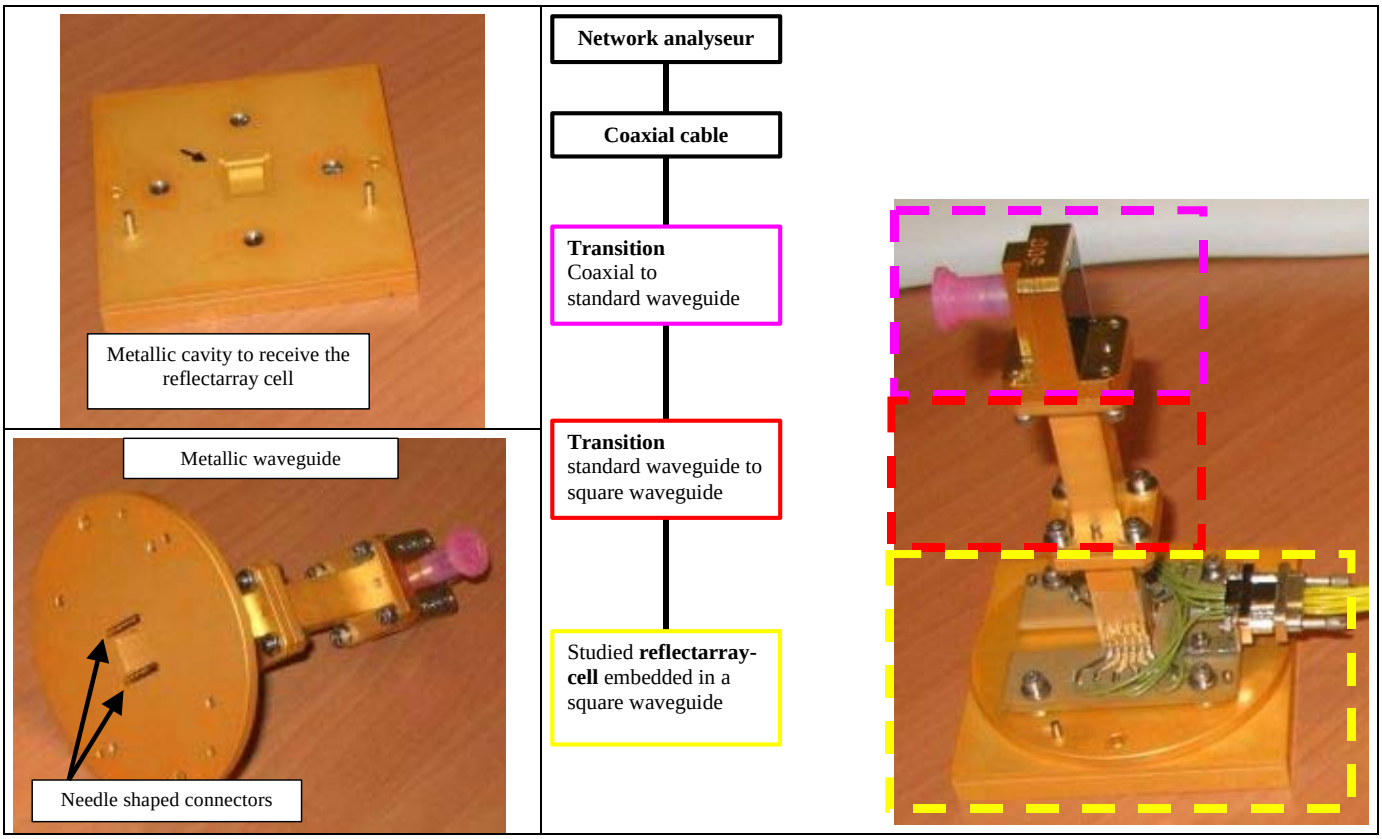

Figure 4.2-2 :Test waveguide device

5. MEASUREMENTS

5.1 PHASE SHIFTER ELEMENT IN KU BAND WITH FROZEN MEMS ON ALUMINA

The engineered cells gave us the opportunity to compare the effect of two kinds of alumina substrates, (one with via holes, the other without via holes), and two kinds of switches topologies, (with MEMS parallel and orthogonal to the line), as described in section 3.1.

Achieved measurements demonstrate :

- firstly that cells with via holes are much better in term of losses ,
- secondly that cells with switch orthogonal to the line are better than cells with switch parallel to the line.

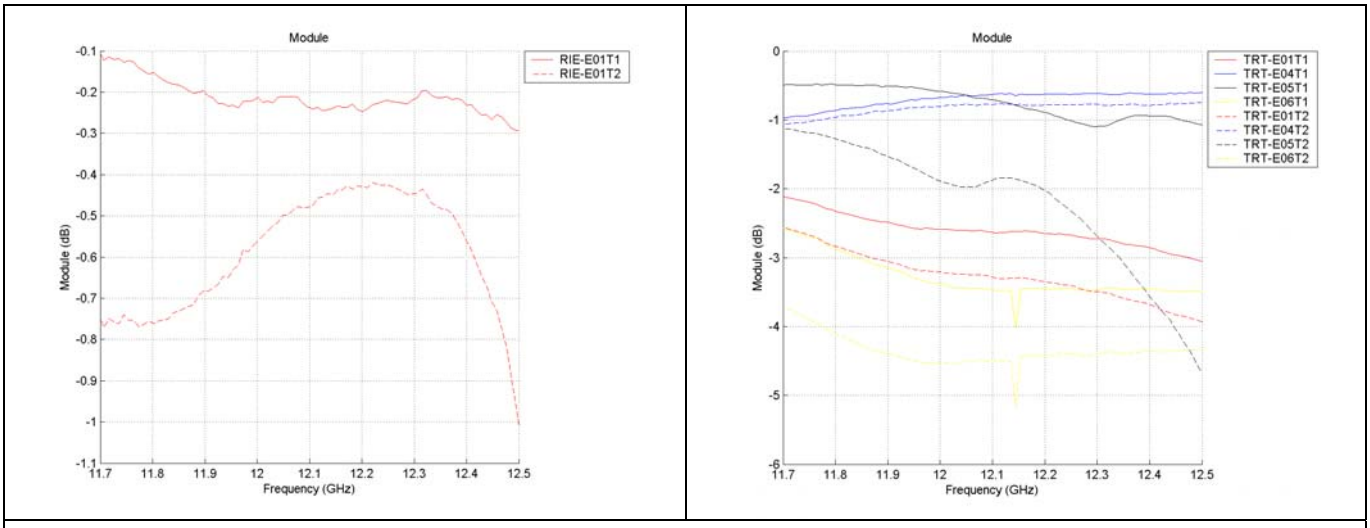

Figure 5.1-1: Module versus frequency for comparison of Type 1 and 2 cells. Both for RIE and TRT type cells.

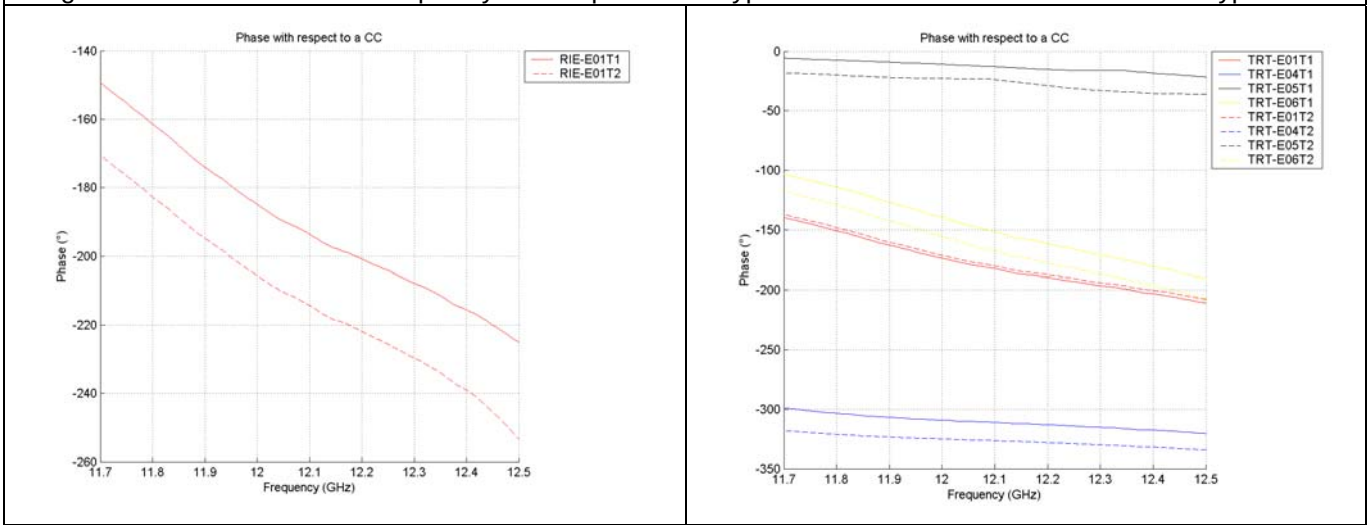

Figure 5.1-2: Phase versus frequency for comparison of Type 1 and 2 cells. Both for RIE and TRT type cells.

As a conclusion we can emphasize that :

- very low losses, less than 0.2 dB, can be reached when both conditions, presence of via-holes and MEMS perpendicular to the line, are met.
- The implanted polarisation lines have no effect on the cell behaviour.

This concerns however only frozen MEMS. A further step would be the design and the measurement of a phase shifter element with fully active MEMS switches.

5.2 PHASE SHIFTER ELEMENT IN KA BAND WITH FULLY ACTIVE MEMS ON MICROMACHINED SILICON

We first measured the three cells without MEMS displayed in the figure below.

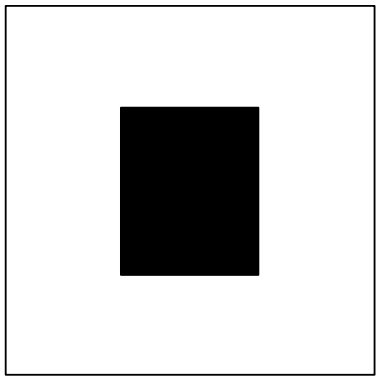

Figure 5.2-1: Patch

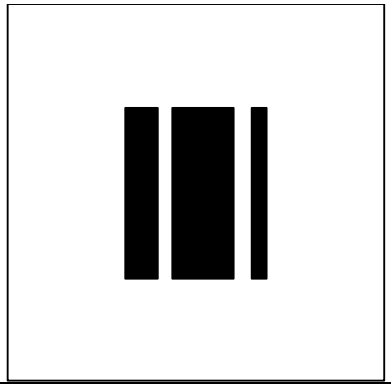

Figure 5.2-2: Opened slots

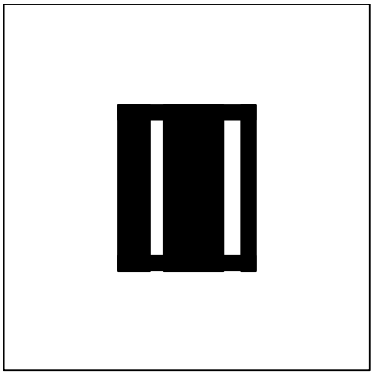

Figure 5.2-3: Shorted slots

The slotted cells exhibited high losses, greater than 1 dB. The patch is the only case were losses remain less than 0,3 dB.

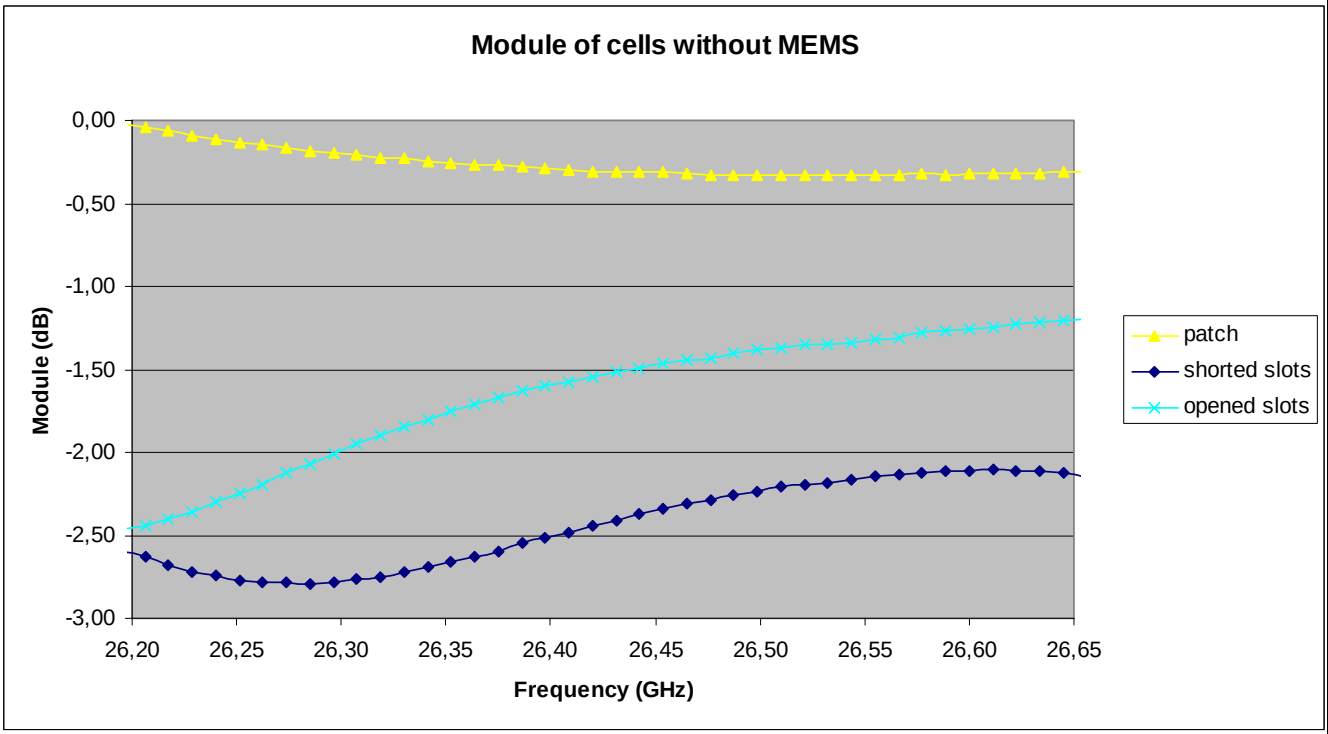

Figure 5.2-4: Measured module of the cell without MEMS.

Losses are assigned to the absence of via holes. The silicon module is greater than the waveguide cavity, in order to be held and also to distribute the DC voltage. As it was not possible to drill via holes in the Silicon, the continuity of the 8mm waveguide cavity could not be enforced. See Figure 4.1-2.

The phase-shift is measured for each cell and compared to a Short-Circuit reference located at the cell position. The measured phase shift was compared to theoretical phase shifts, computed for variable thickness of the remaining Silicon membrane. We can deduce from Figure 5.2-5 that a satisfactory comparison between theory and experiment is achieved, provided we assume the thickness to be around 20 μm. This was confirmed by a measurement of the membrane thickness performed with an optical profiler at LAAS. A 22μm thickness was measured.

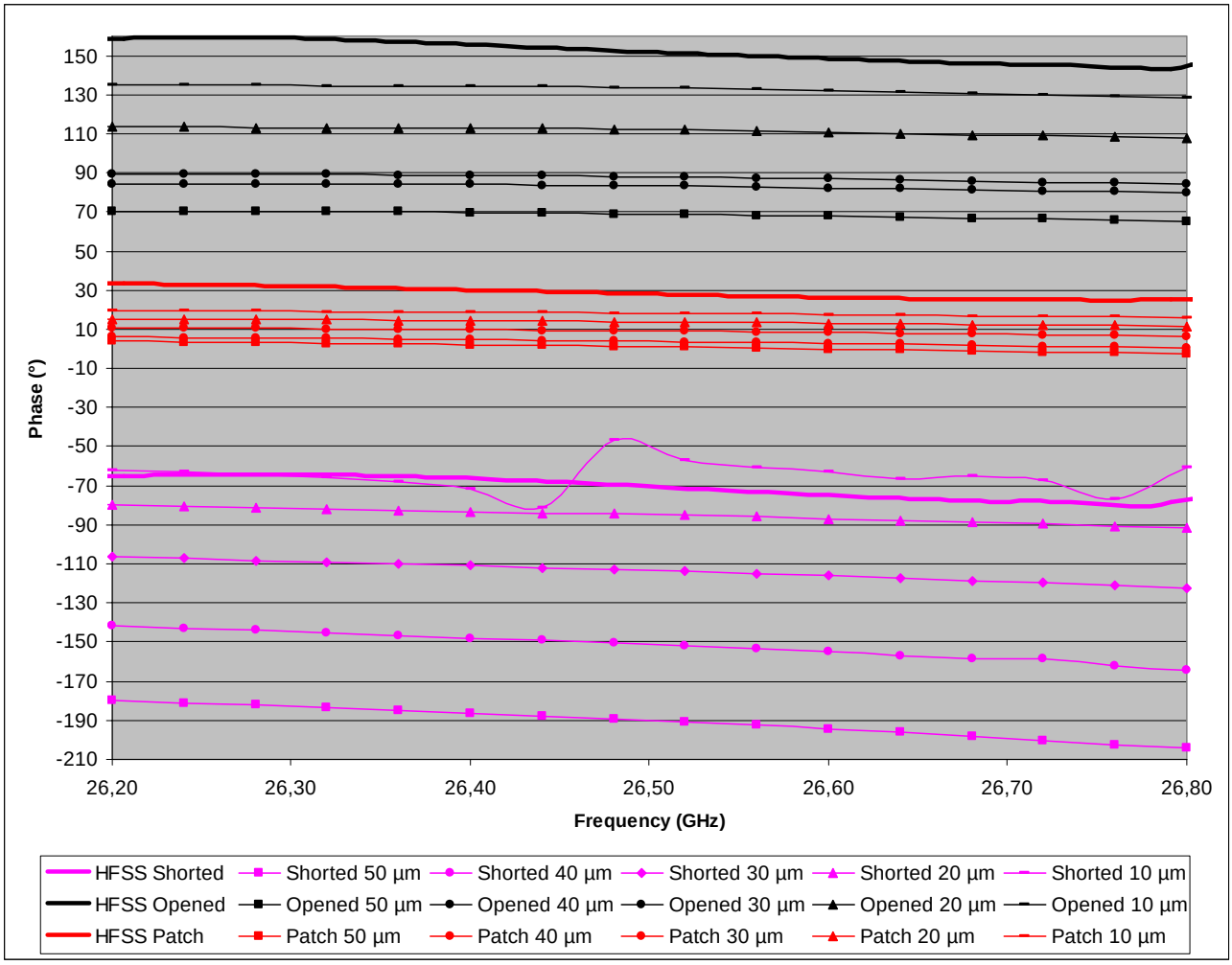

Figure 5.2-5: Measured results of the phase compared to predicted results

We first focus on cells to be compared with the passive elements studied in the previous section. The patch case (Figure 5.2-1) is identified to the case of a cell with all MEMS in down position (Figure 5.2-6); the case with opened slot (Figure 5.2-3) is identified to the case of a cell with all MEMS in up position (Figure 5.2-7); the case with shorted slot (Figure 5.2-3) is identified to the case of a cell which has its side MEMS in down position (Figure 5.2-8).

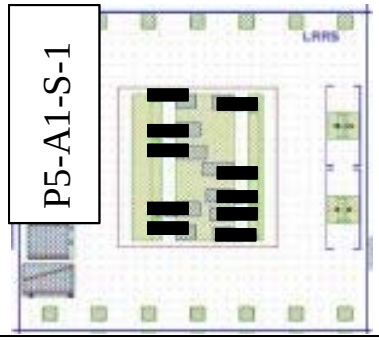

Figure 5.2-6: Case identified to the patch case

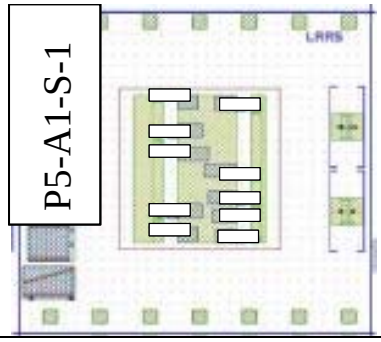

Figure 5.2-7: Case identified to the opened slot case

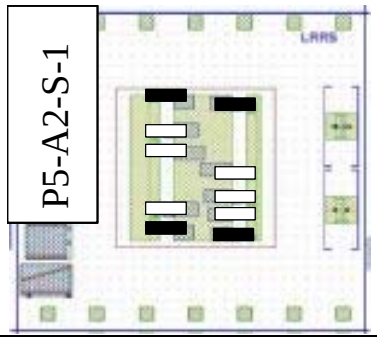

Figure 5.2-8: Case identified to the shorted slot case

As shown in Figure 5.2-9 and Figure 5.2-10, the patch element has similar losses than the cell with all the MEMS in down position. The phase shift for both cases are also very similar. This seems to indicate that the MEMS in down position realise real short circuit. The behaviour is therefore nominal.

Conversely, the slotted patch designs present different losses and phase shifts than their counterpart cell with MEMS. This indicates that the MEMS in up position affect significantly the behavior of the slot.

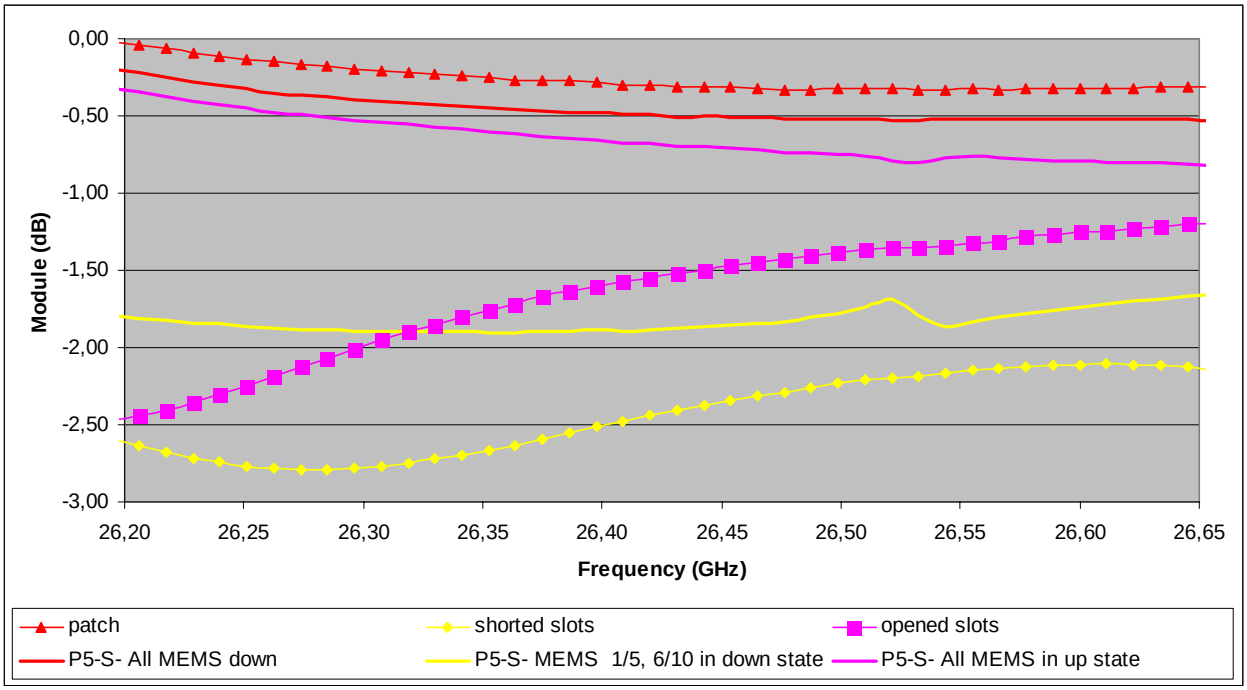

Figure 5.2-9:Comparison between patch elements and cells with frozen MEMS (losses)

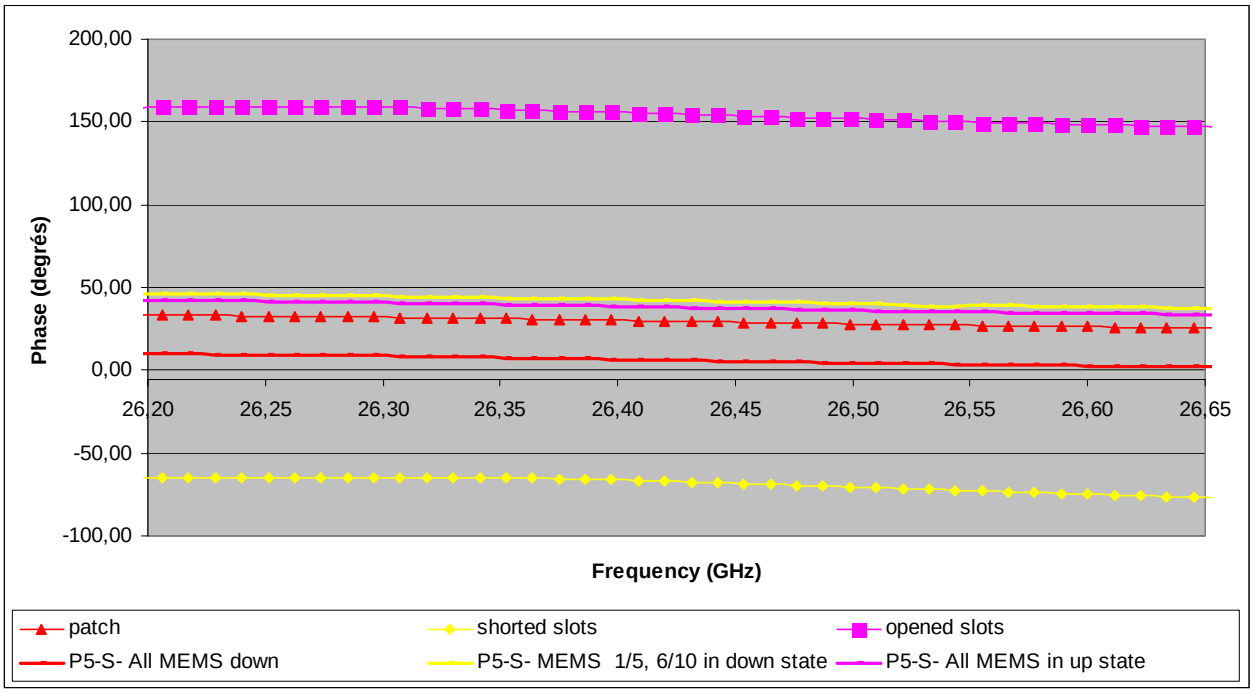

Figure 5.2-10: Comparison between patch elements and cells with frozen MEMS (Phase shift)

An explanation was provided by a parametric study on the capacitance.

The first simulation considered C_{down}=1.2 pF, . For C_{up}=20 fF (C_{down}/C_{up}=60), the range of predicted phase shifts offered by the three cells is poor : Around 30°. This is exactly the range of phase shift which is effectively measured.

Besides, for an infinite ratio between C_{down} and C_{up}, a large phase shift range is achieved : +140° for the equivalent shorted slot design, +240° for the equivalent open slot design. This phase difference is compared to that obtained for the passive elements (Figure 5.2-5) : +120° for the shorted slot design, +290° (or -70°) for the open slot design. This shows that for these values of capacitances, the cells with frozen MEMS recover their expected behavior. The cell with all frozen MEMS in down state (Figure 5.2-6) is equivalent to the passive patch element (Figure 5.2-1); the cell with all MEMS in up position (Figure 5.2-7) is equivalent to the opened slot element (Figure 5.2-3); the cell with its side MEMS in down position (Figure 5.2-8) is equivalent to the shorted slot element (Figure 5.2-3).

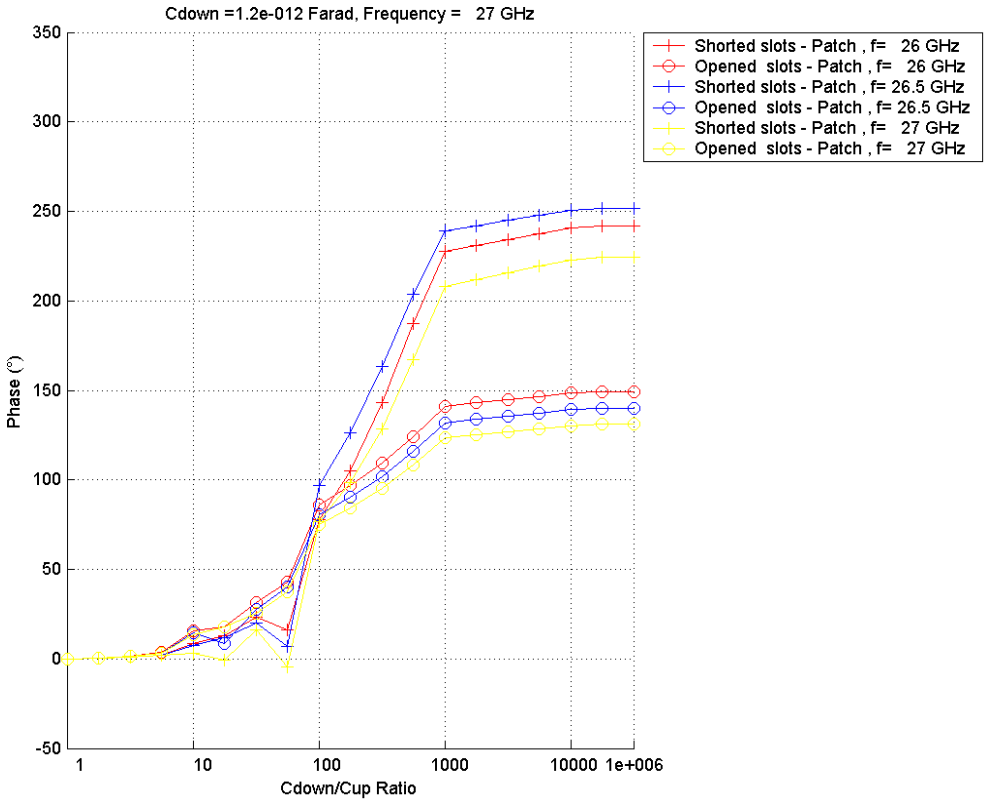

Figure 5.2-11 : Predicted phase shift range offered by the slotted cells with frozen MEMS as a function of the MEMS capacitances in down or up states. C_{down} =1.2 pF
The equivalent patch cell (Figure 5.2-6) is taken as reference

The real capacitances are therefore not matched to the design. The simulation showed that a ratio greater than 1000 would have been necessary; i.e. a capacitance in up state close to 1 fF.

This parametric study demonstrated the importance of the MEMS loading on the design. This study was not carried out during the design stage. At this stage, only HFSS was available, and its simulations did not converge. The simulations were then performed after the multiscale EM tool was delivered.

Now, this study calls for a modification of capacitances for an updated run. Specifications of 1fF for the up capacitances ensure no problem of operation for the reflectarray element, as seen above. However, such a high capacitance seems then very difficult to obtain and it is more rational to plan 5fF up capacitance, with some updates on the RF designs.

5.3 SYNTHESIS

On the phase shifter elements made on alumina substrate, with frozen MEMS, excellent agreement between theory and measurements was observed. These breadboards were manufactured with bias management. This shows that the bias management was well designed,

since it has no effect on the RF characteristics of the phase shifter elements. Finally, the losses measured for these breadboards were very reduced (lower than 0.2 dB).

Breadboards on bulk-micromachined Silicon were also manufactured and tested. Good mechanical actuation was observed. RF tests were also performed on test structures in order to derive the performances of the MEMS switch. However, the RF characteristics of the phase shifter elements were not fully satisfactory : Losses were measured and suspected to be due to the absence of via-hole. Besides, a poor phase shift range was measured. The explanation was provided thanks to the multiscale EM tool. Simulations demonstrated very good agreement with measurements and showed that the capacitance of the MEMS in up state was too high.

Second runs with fully active MEMS switches for the alumina cases, and with designs with updated capacitance values for the Silicon cases, would be a logical follow-àn of this first benchmark study.

6. PERSPECTIVES

A powerful reflectarray phase shifter element has been designed, which offers high phase resolution, manufacturing moderate complexity once the technology has been developed.

Promising results were obtained with Frozen MEMS on Alumina, which demonstrated that low losses could be achieved. Phase shifter elements with fully active MEMS switches were also developed on micromachined Silicon, with satisfactory agreement between experiment and theory. However, updates of design is required to operate with lower capacitances.

The idea for a further benchmarking study is to benchmark MEMS switches, novel materials, innovative solutions for packaging in the environment of a reflectarray element. This will be much more representative than a typical test of a MEMS on a coplanar waveguide. No major RF design updates is requested for this activity. The element has already been optimised, and it is believed that the change of MEMS, materials, packaging solutions will have only a minor effect.

This case will be proposed under a common ACE2/AMICOM activity.

Two options are proposed :

- MEMS switches are manufactured as single components, and are mounted on the reflectarray elements (etched on either PCB or Alumina, or any alternative material of interest)

- MEMS switches and the reflectarray elements are manufactured on the same substrate, according to a monolithic approach. This substrate shall then be low loss.

The new activity will include the following tasks :

- Selection of the novel MEMS switches topology, novel materials, novel packaging solutions,… to benchmark. Major constraints such as the characteristics of the substrate (effective permittivity, its minimal thickness, resistivity,…), the characteristics of the MEMS switches (Typical Up to Down Capacitance ratio, equivalent circuit, dimensions, …) will be provided to the RF designer so that the element RF definition can be updated if necessary ;

- Update of the original layout in order to accommodate the MEMS switches and the bias circuit within the reflectarray elements. Suggestion of design modification to complete the MEMS accommodation, and discussion with the RF designer in order to state whether these changes are acceptable ;

- For the monolithic approach, Manufacturing of the MEMS based element module ;

- For the component approach, Manufacturing of the MEMS packaged switch and of the reflectarray element, and mounting of the component on the reflectarray element ;

- Test of the reflectarray element ;

END OF DOCUMENT

Activity 2.1.3 Benchmarking Cases

European Commission - 6th Framework Programme	***ACE (Antenna Centre of Excellence)***	Information Society Technologies

BENCHMARKING CASE ON PRINTED ANTENNA ARRAY IN 60 GHZ BAND MULTILAYER TECHNOLOGY AND THICK GROUND PLANE

INSTITUTION : IETR
AUTHORS : O.LAFOND, M.HIMDI
REVISION : V0, DATE : 06/12/05

Activity 2.1.3 Benchmarking Cases

I. Introduction

Microstrip technology is attractive at these frequencies if one uses material with weak losses and a low cost technology. Glass Teflon alias RT/D Duroïd 5880 or Polyméthyl – Pentène alias TPX are good candidates. But spurious radiation due to the feeding network often occur in the millimeter band. These effects often increase the cross polarisation component and the sidelobe level. A solution to reduce these problems is to use slot coupled printed antenna arrays, with the radiating elements which are separated from the feeding lines by the ground plane. Various types of pattern have been investigated, either directive or on the contrary with large sector beam.

II. Details about technologies

An aperture coupled microstrip patch antenna [1] is represented on figure 1 with two different substrate layers. Several examples of aperture coupled microstrip patch antennas have been realized in millimeter waves at 40 GHz [2], 77 GHz [3] and 92 GHz [4]. Good results have been obtained but the realisation methods are a little bit complex because two different substrates are used, one with a high permittivity(GaAs) for the feeding lines and the other with a lower permittivity (Quartz ..) for the radiating elements. In this article, a different solution compatible with MMIC integration using a thick ground plane is presented to realise some antenna arrays with the same substrate for the two layers. We test it for different kind of substrates, the Glass Teflon (RT/D Duroïd 5880, ε_r = 2,23, h = 0,127 mm) for the first technologies and the TPX (Polyméthyl – Pentène, ε_r = 2,17, h = 0,127 mm) for the last one which has been developed in collaboration with a local company (Avi & Peschard) in France [5].

These two technologies are explained on figure 2a with Glass Teflon which is a laboratory technology development and on figure 2b for with TPX (Avi&Peschard). For both technologies a thick ground plane (0.2mm) has put between the bottom and top substrate layers.

With the Duroïd (figure 2a), the initial copper film is first removed and after the two substrate layers are stuck and pressed at high temperature. For the TPX realisation (figure 2b), several sheets of substrate are stacked and pressed at high temperature to obtain the TPX correct thickness. In millimeter waves (60 Ghz here), the thickness of ground plane becomes important versus wavelength and it become primordial to take it into account to improve the prediction of the antenna's input impedance [6, 7, 8].

In term of techniques to engrave slot into ground plane, different solutions exist : classic chemical etching is possible if thickness is not so strong, mechanical technique, electro-erosion or laser patterning. In the precedent cases, chemical etching has been used because all the circuits have been manufactured with the same technique. Dispersion exist between the slot size due to this classical etching

process but experimental results show good agreement with prediction for printed antenna arrays (linea arrays composed of 6 patches or two dimensionnal antenna array composed of 36 patches).

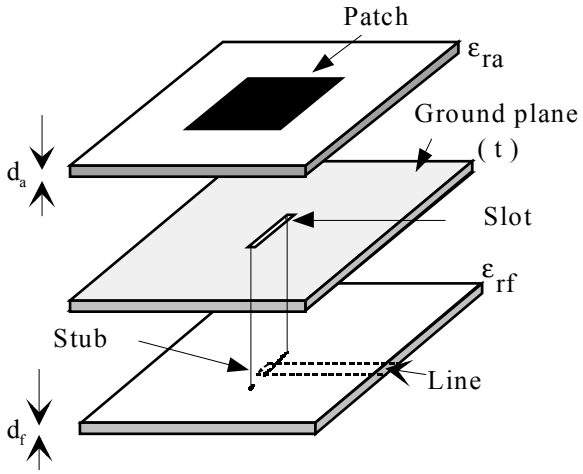

Figure 1 : Aperture coupled patch antenna

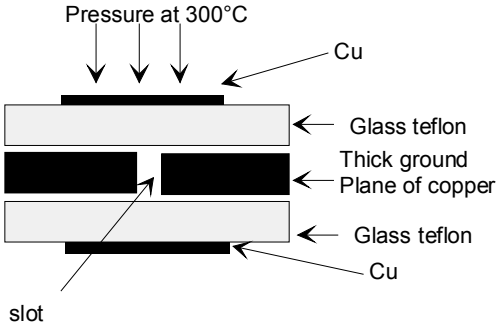

$\varepsilon_r = 2{,}23 \pm 0{,}015$, tg $\delta = 4^e$-03,

Figure 2a : Glass teflon technology

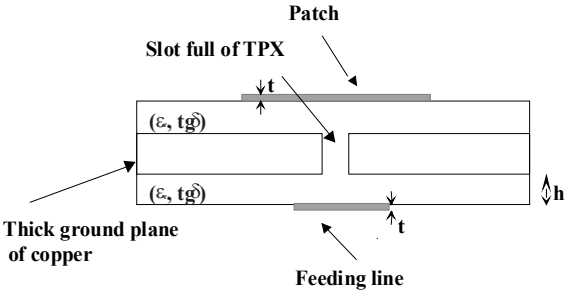

$\varepsilon_r = 2{,}17 \pm 0{,}015$, tg $\delta = 4^e$-03,

Figure 2b : TPX technology

III. Prototypes and results

First, a 6 patches linear printed antenna array has been optimsed with both technologies and results are compared in 60 Ghz band. The typicall prototype is presented on figure 3a for radiating elements and 3b for feeding line network.The patches have been tapered to reduce the sidelobe level up to -20 dB below the main beam. Each patch is electromagnetically exists by line via a thick slot engraved in the ground plane.

Figure. 3a : radiating elements face
spacing between patches : 0,72λ0

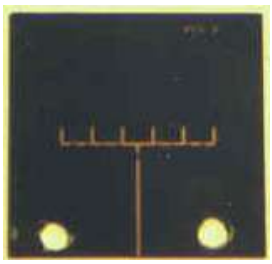

Figure 3b : Feeding network
Amplitude taper : (0.3; 0.7, 1, 1, 0.7, 0.3)

In the following table, characteristics of patches and slot (sizes) are given for both technologies. In the two cases, the width of slot equals 0.2 mm.

Substrates	ε_r	Substrate thickness	Square patch	Slot length
Glass teflon (Duroïd)	2,23	0,127 mm	1,28*1,28 mm^2	0,92 mm
TPX	2,17	0,127 mm	1,32*1,32 mm^2	0,85 mm

The measured radiation patterns at 59,5 GHz in the H-plane are compared on figure 6a et 6b for the two antennas. The obtained results are very closed for these two arrays. The same cross polarisation level is measured, 27 dB below the main beam, and the same beamwidth (14,5°) and efficiency (55%).

In order to get a pencil beam, a two dimensional antenna array with 36 patches (6*6) has been designed.. The figure 5a et 5b represent the two sides of this array which has been made with the TPX. The radiating elements are identically tapered in amplitude in both the E and H planes to reduce the side lobe level. The radiated patterns in co and cross polarisation are given at 59 GHz on figures 8a (E plane) et 8b (H plane). The beamwidth in the E plane and H plane are respectively equal to 15° and 16°. The cross – polarisation level is lower than –27 dB in the two planes. The side lobe level is around –22 dB in the E plane and –20 dB in the H plane. The efficiency of this array is around 40 % at 59 GHz (power gain around 17,5 dB).

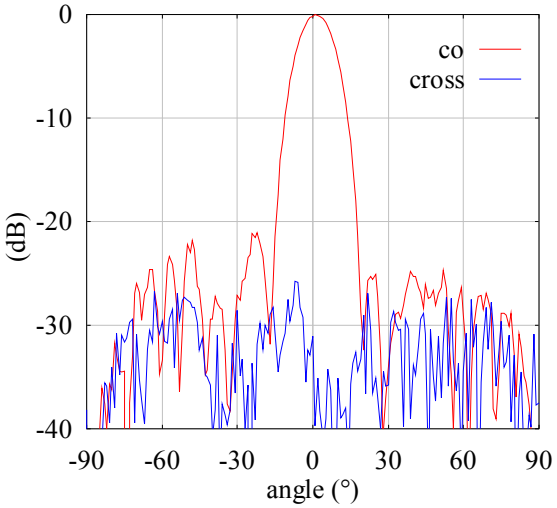

Figure 4a : Glass teflon technology

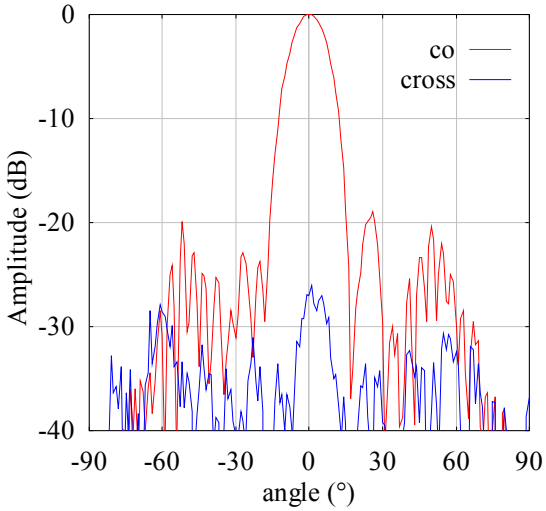

Figure 4b : TPX technology

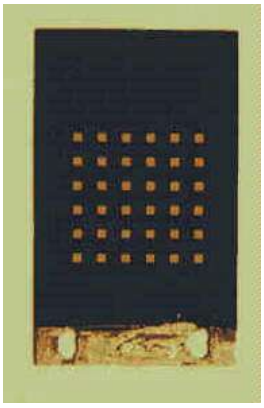

Figure 5a : Radiating array
spacing between patches : 0,72 λ_0

Figure 5b : Feeding lines network
Amplitude taper : (0.3; 0.7, 1, 1, 0.7, 0.3) in the two planes.

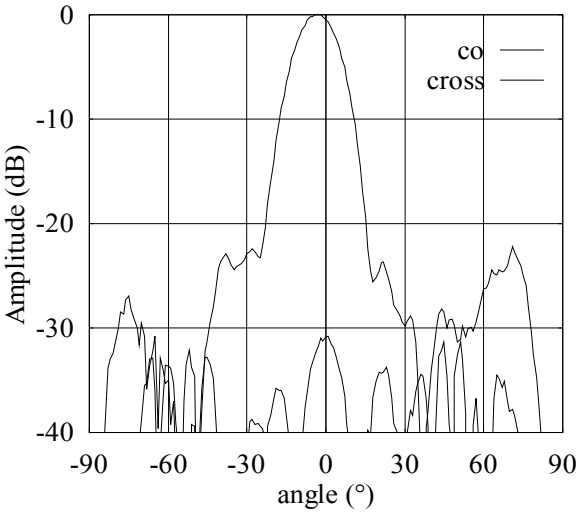

Figure. 6a : E plane at 59 GHz

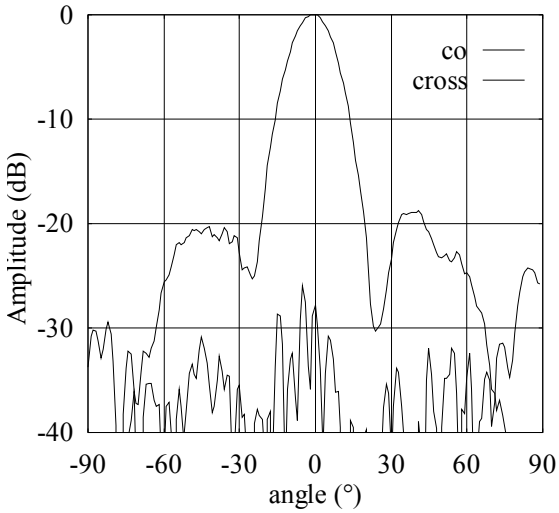

Figure. 6b : H plane at 59 GHz

IV.Conclusions

Two multilayer technologies using thick ground plane have been shown and allow to separate feeding layer from radiationg one. The principal adavantage is to have the possibility to realise active antennas with out spurious radiation on active devices (MMIC or MEMS). Active antennas have also been manufactured with LNA for example in 60 Ghz band. Moreover, it is also possible to realise mettalized holes with theses techniques. Thus, different substrates can be used for active layer and radiating layer. For example an active reconfigurable antenna for directivity diversity is under test and in this case feeding lines are printed on RT/Duroid 3003 and patches on RT/Duroid 5880.

V. References

[1] : D. M. POZAR, 'A reciprocity method of analysis for printed slot and slot – coupled microstrip antennas', IEEE Trans. Antennas Propagat, vol.AP – 34, pp. 1439 – 1446, Dec. 1986.

[2] : H. OHMINE, T. KASHIWA, T. ISHIKAWA, A. IIDA and M. MATSUNAGA, 'An MMIC Aperture coupled Microstrip antenna in the 40 GHz band,' Proceedings of ISAP, pp. 1105 – 1108, 1992.

[3] : M. STOTZ, G. GOTTWALD, H. HASPEKLO and J. WENGER, 'Planar millimeter Wave Antennas using SiNx Membranes on GaAs', IEEE Transactions on Microwave Theory and Techniques, Vol. 44, N°. 9, September 1996.

[4] : A. IIDA, M. HIEDA, K. ITOH, H. OHMINE, K. MATSUO, T. FURUYA and T. KASHIWA,' A 100 GHz – Band antenna Stacked Monolithic Receiver using Multilayered Configuration', Proceedings of ISAP' 96, Chiba, Japan.

[5] : AVI&PESCHARD : ZAC de la Goulgatière, 35000 Châteaubourg, France.

[6] : O. LAFOND, M. HIMDI, J.P. DANIEL : 'Aperture coupled microstrip patch antenna with a thick ground plane in millimeter waves', Electronics Letters, August 1999, Vol. 35, No. 17, pp 1394-1396.

[7] : M. HIMDI, O. LAFOND, S. LAIGNER and J.P. Daniel : 'Extension of cavity method to analyse aperture coupled microstrip patch antenna with thick ground plane', Electronics Letters, August 1998, Vol. 34, No. 16, pp 1534 – 1536.

[8] : O. LAFOND, M. HIMDI, J.P. DANIEL : 'Slot coupled millimeter printed antenna arrays (60 GHz)', Millennium Conference on Antennas and Propagation, AP200, Davos, Switzerland, 9 – 14 April 2000.

European Commission - 6th Framework Programme	***ACE (Antenna Centre of Excellence)***	Information Society Technologies

Benchmarking Case on 30 GHz Patch Antennas

Institution	**Authors**
Univ Birmingham	Ee LEE, Peter GARDNER, Peter HALL

Document Evolution		
Revision	Date	Reason of change
0	28-11-05	

TABLE OF CONTENTS

1. Objective

The objective of this section is to describe the design and fabrication of single and dual polarised patch arrays fabricated using precision chemical etching, in order to provide an example of the capabilities and limits of that technology.

2. Manufacturing Details

The antenna modules described here were manufactured by Optiprint (http://www.optiprint.ch/) to designs generated at Birmingham University.

The etching tolerances provided by Optiprint are dependent on a number of factors. This is highlighted in the graph shown in figure 1. The effect of the copper thickness has a significant impact on the accuracy achievable through chemical etching. For greater control of the etching tolerance, a substrate with minimum copper thickness is preferred (eg. 18 um for mm-wave designs). As stated in their design file, the standard etching accuracy is about +/-35 um.

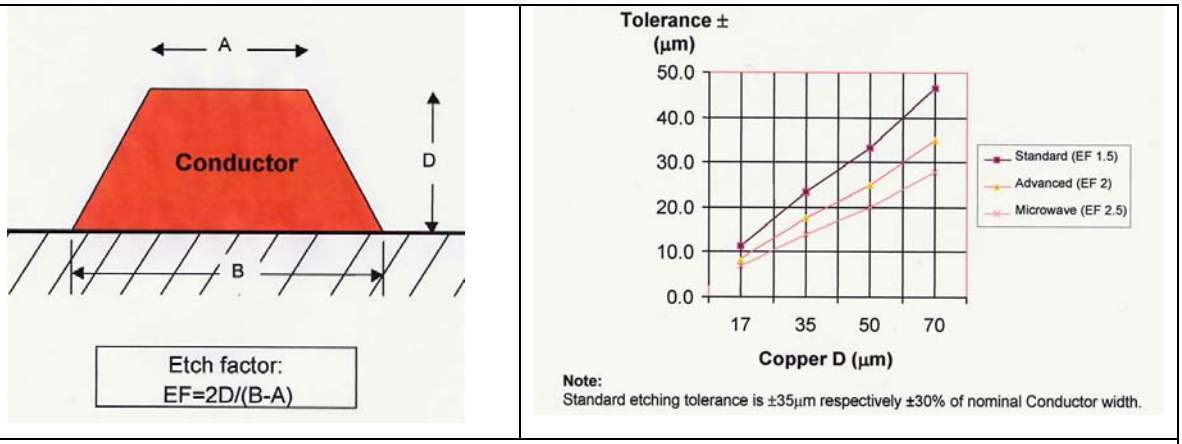

Figure 1

3. Design and Measurement Details

For a RT Duriod 5880 substrate with a thickness of 0.254mm, simulation with HFSS suggested that a patch antenna operating at 32 GHz will have a resonant length of about 3mm. Figure 2 shows the physical layout for a single patch antenna and Figure 3 shows its simulated return loss performance.

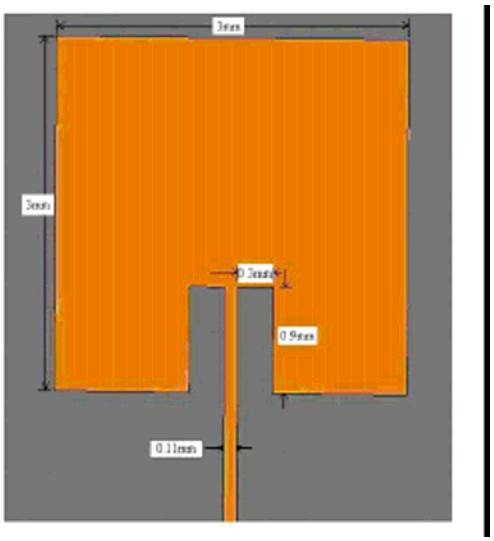

Figure 2: Single Element patch design

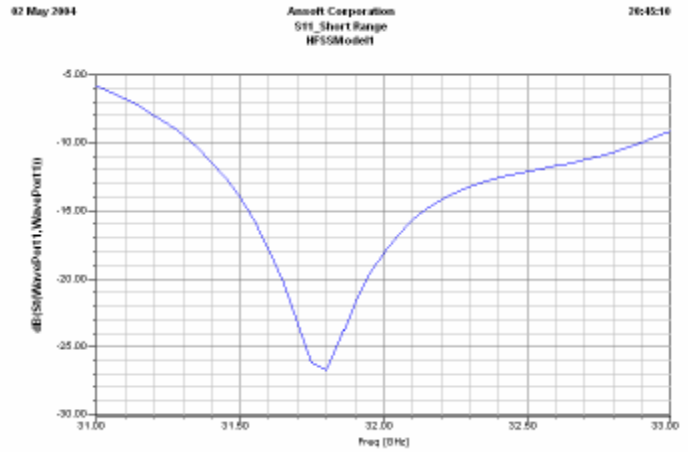

Figure 3: Simulated Return Loss of Single Polarized Sub-array

From this initial simulation, a number of antenna sub-arrays have been built as shown in figure4.

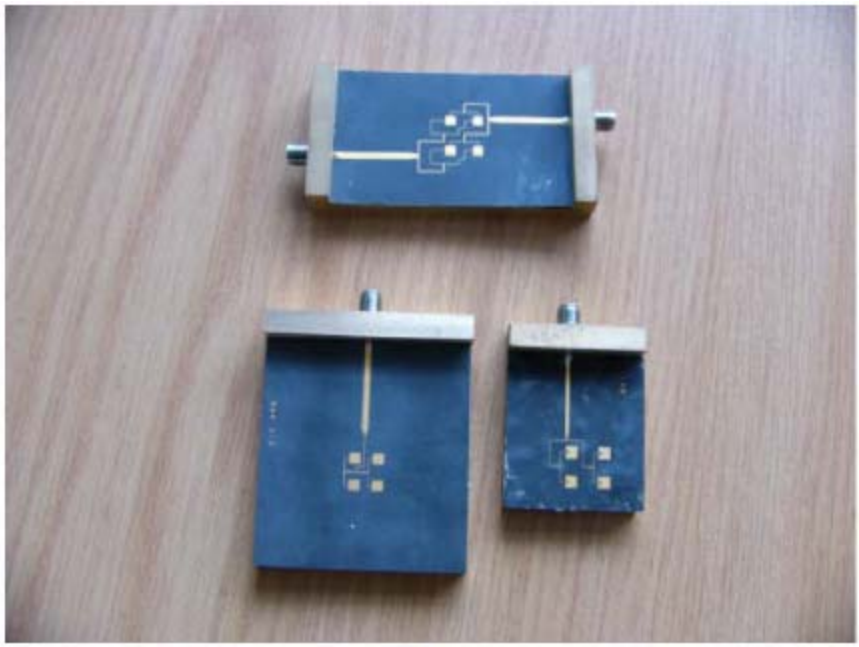

Figure 4: Manufactured 32 GHz mm-wave antenna

3.1 Single Polarised sub-array

The single polarised sub-array design is based on the use of a 0.254mm thick Duroid 5880 substrate. The design of 2×2 SP sub-array with corporate feed is shown in Figure 5. Microstrip feed lines are used, for simple planar structure and easy performance prediction. A pure planar structure is desirable for the final complete array, for the ease of housing configuration and alignment. The simulation of the single polarised sub-array shows promising performance. Several key parameters are listed in the following diagram. Figure 5 shows the computed input return loss. The centre frequency is about 31.8GHz, and the –10 dB bandwidth is about 1.4GHz (from 31.4GHz to 32.8GHz). The 3D gain plot, which displays the 3D radiation patterns is also given. It can be seen that the gain in the peak direction is above 12dBi. Note that the Phi=0 plane is the X-Z plane. The patch antenna is placed in the X-Y plane, with the antenna facing the positive Z direction.

	Simulated
Resonant Frequency (GHz)	31.8
Bandwidth (GHz)	1.4
Gain (dBi)	12
Efficiency	85%
Beamwidth (degree)	>15

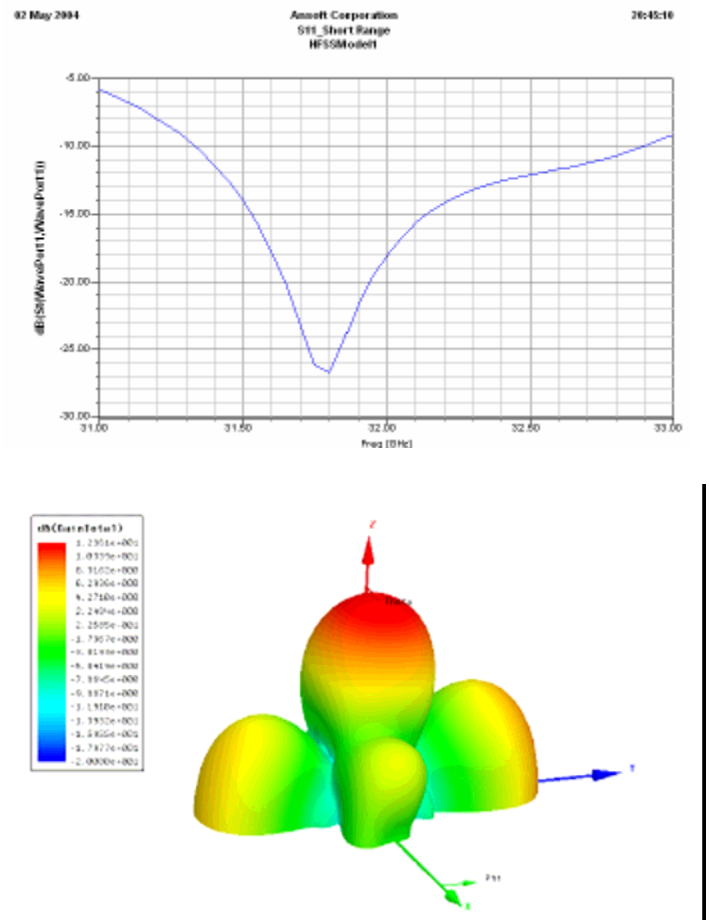

Figure 5: Simulated result for the single polarised microstrip sub-array

The following diagram shows the measured return loss performance. Comparing the measured and simulated results, the centre frequency was observed to shift down by about 1.65GHz, which is about 5.2% of 31.8GHz. The simulated bandwidth was 2.3 times greater than that measured. Although the required bandwidth is 300MHz which is met without doubt, the bandwidth difference between the predicted and the actual result is large. Radiation patterns were measured, as shown in Figure 7. These measurements were taken at 30.077GHz. The beamwidths in both E and H plane are larger than 10 degrees. The major beam in E plane tilts about 5 degree. This is possibly caused by misalignment of the two antennas in experiment. As shown in Figure 8, the gain in Co-polar and Cross-polar orientations were measured. The absolute values of the gain were obtained after comparing with the standard 20dB gain horn antenna. The difference of co and cross polar is about 10dBi at 30.1GHz.

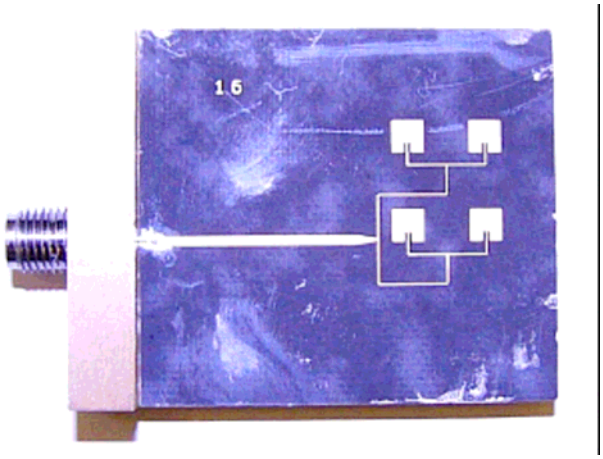

Figure 6: Enlarged Photo of inset feed single polarized sub-array

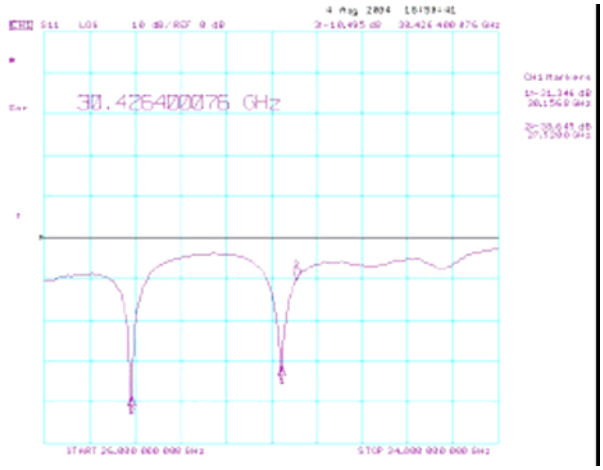

	measured	simulated
resonant frequency (GHz)	30.15	31.8
bandwidth (GHz)	0.6	1.4

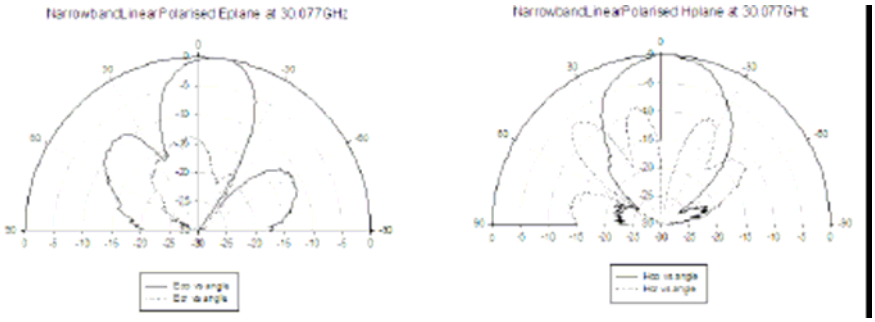

Figure7: Measured return loss and radiation pattern for a sinlge polarized sub-array

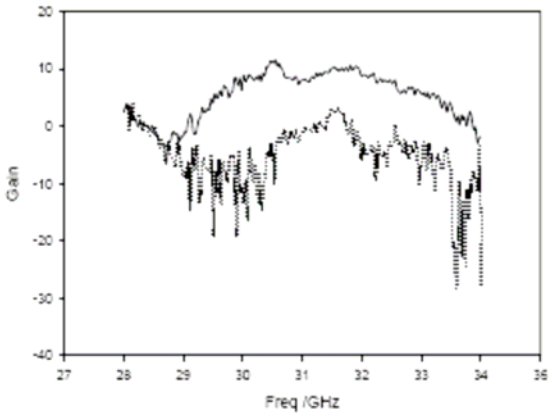

Figure 8 Measured Gain of Narrowband Single Polarized Sub-array
(Solid Curve is Co-polar Gain, Dashed is Cross-polar Gain)

3.2 Dual Polarized Sub-array

From the single polarized antenna design, an additional horizontal feed was added to each patch to create a dual polarized (DP) sub-array. This is shown in figure 9. Inset feeding at the patch was not possible because it would create an uneven structure, affecting the isolation between the two feeding networks and decreasing isolation between the two polarizations. Figure 9 shows the initial design layout. For the ease of routing feed lines, orthogonal stepping lines were used. In this way, phase difference is easy to adjust and the routing at the centre of the four elements is able to maintain a good isolation. The simulation results of initial design of dual polarized sub-array came from 3 simulations. The sub-array antenna layout in these 3 simulations are the same, the only differences are in the configuration of the feeding port. Simulation 1 was done with port 1 fed only. Although the horizontal feeding network exists, there was no excitation port on that side of the structure. Simulation 2 was done with port 2 fed only. Simulation 3 shows the results of feeding at both ports simultaneously. The purpose of simulation 3 is to find out the isolation between two ports: S_{12} and S_{21}. Simulation 1 and 2 show the return loss and radiation pattern in each polarization. The simulation performances of this initial design indicate it meets most of the project requirements. But the cross polar performance when feeding at port 2 is a little bit weak, as shown in Figure 10. The difference of co and cross-polar in the beamwidth is just above 7dB. The weak cross-polar performance when feeding from port 2 came from scattering of surface waves. This is due to the relatively thick substrate and too many bends in feeding network. Redesigning the feeding network to eliminate unnecessary bends), is expected to improve the co-polarisation performance of the antenna.

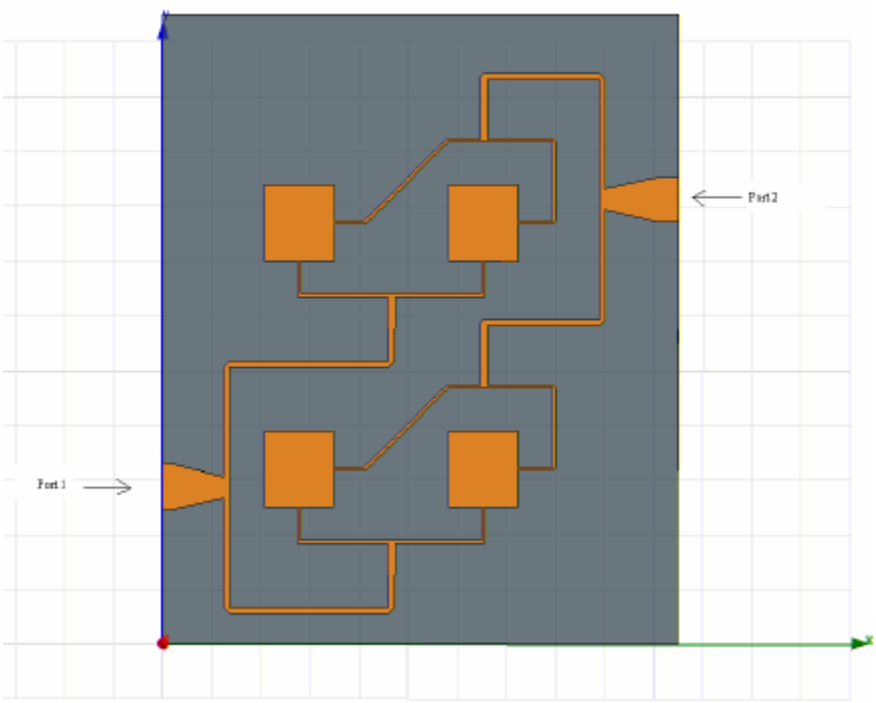

Figure 9: Initial dual polarized sub-array

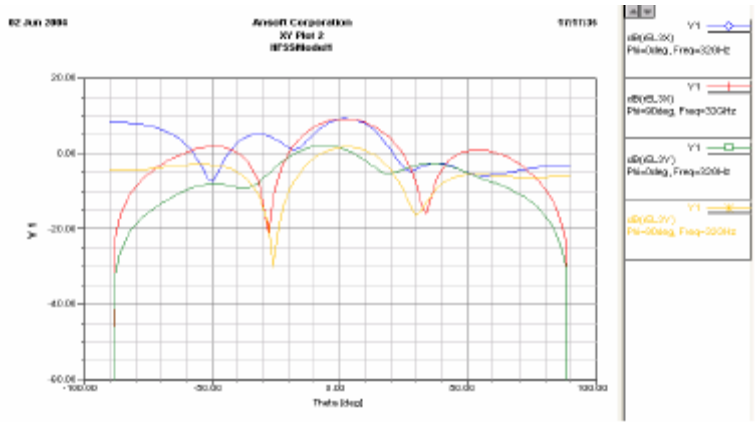

Figure 10: Calculated Radiation Patterns Feeding at Port 2 at 32GHz
(co-polar blue, phi = 0°, red, phi = 90°; cross-polar green, phi = 0°, yellow, phi = 90°)

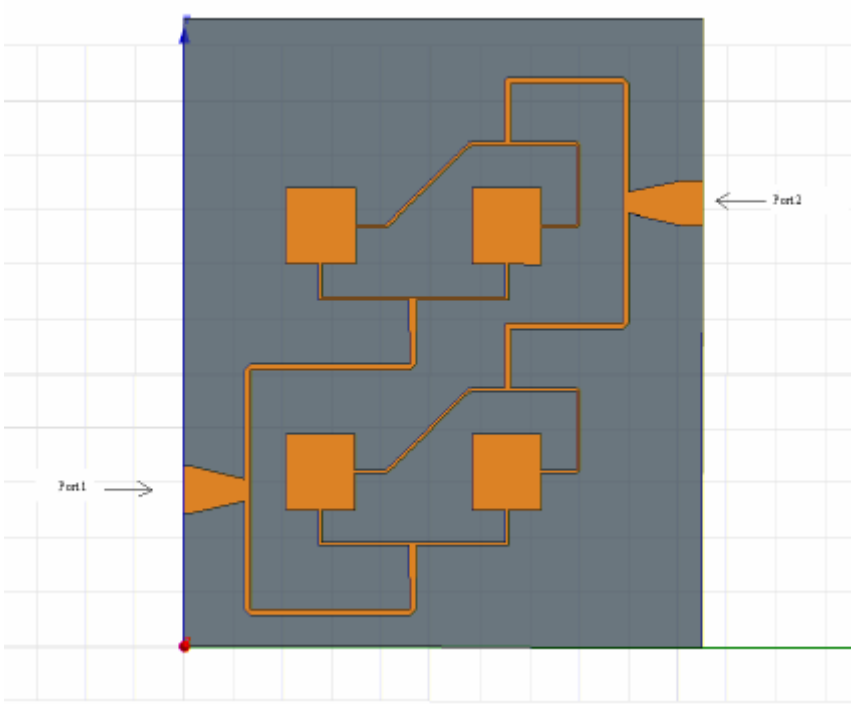

Figure 11: New iteration of the dual polarized sub-array antenna (Not yet tested)

Summary of Results for Initial Design of Dual Polarized Narrowband Sub-array Antenna	
Port 1 (polarized in Y direction):	
Center Frequency	31.6GHz
Bandwidth	1.7GHz (30.8GHz – 32.5GHz)
Gain	about 11.7dBi
Beamwidth	> ±10°
Radiation Efficiency	about 96%
Co – Cross Polar in beamwidth	> 10dB
Port 2 (polarized in X direction):	
Center Frequency	31.95GHz
Bandwidth	1.2GHz (31.3GHz – 32.5GHz)
Gain	about 12.4 dBi
Beamwidth	> ±10° tilts about 2 degree
Radiation Efficiency	about 93%
Co – Cross Polar in beamwidth	about 7dB
Common Bandwidth	about 1.2GHz
Isolation in common band	about -17dB

- 35 -

Table :Simulation result for the dual polarized sub array

The measured return loss of the initial design is shown in Figure 12. The diagram below shows the resonant frequency and bandwidth comparison between simulation and measurement. It can be seen from the tables that the centre frequencies are all shifted down about 1GHz, about

3.2%, which also happens to our single polarized antenna measurement. Again, the bandwidths were over-predicted, 2.09 % for port 1, and 5% larger for port 2. The very limited bandwidth difference at port 2 is very interesting, and need furthers discussion. The measured common band is about 800MHz, comparing to 1.2GHz from simulation. The coincidence of the bandwidth and centre frequency of the two ports shows good matching at both side of the feeding network. The measured radiation pattern of vertical polarization (fed at port1) is shown in Figure 12. These measurements were taken at 30.6GHz. The beamwidths in both E and H plane are larger than 10 degrees. Within the major beam, the cross polarization level in E plane is below -10dB relative to the co polar. In the H plane, it is also below -10dB in the -10 to +10 degree beam. As for radiation patterns of horizontal polarization, preliminary measurements confirmed the high cross polarization problem. The difference between cross and co polar in the H plane is about -5dB. And because of scattering surface wave at those bends, spurious radiation was observed in the measurements. The predicted radiation patterns of all these designs agree well with the measurements. In the final design the number of bends in the horizontal polarized feeding network has been reduced. This solved the high cross-polar problem in the simulation.

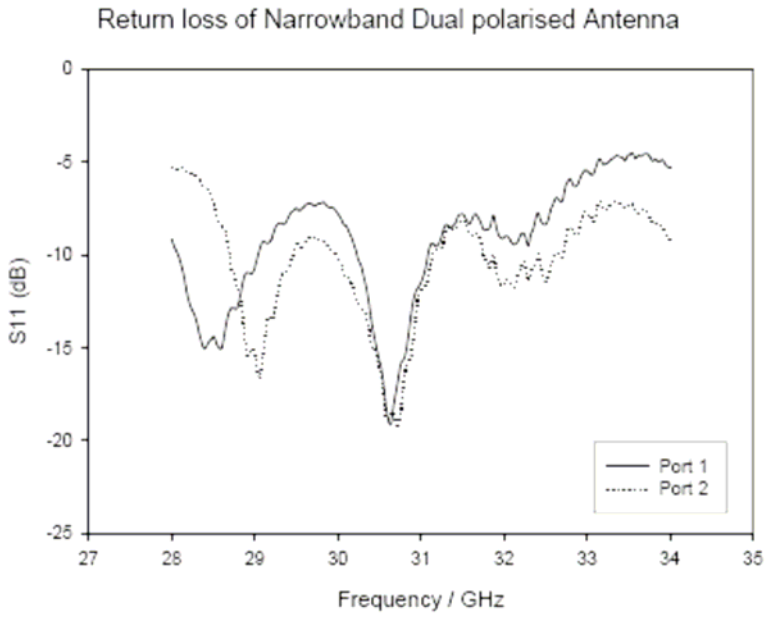

	Port1		Port 2	
	measured	simulated	measured	simulated
resonant frequency (GHz)	30.64	31.6	30.70	31.95
bandwidth (GHz)	0.81	1.7	1.14	1.2

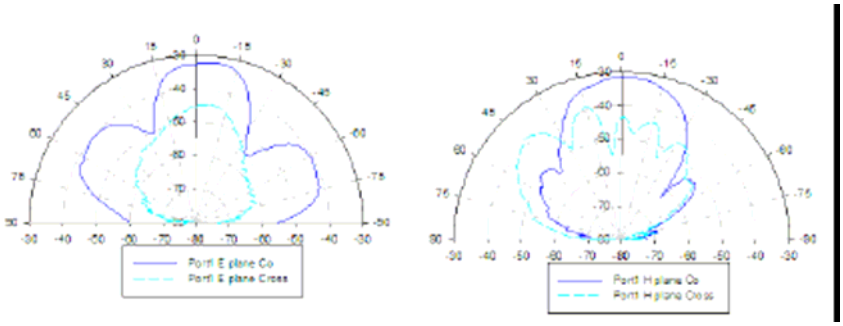

Figure12: Measurement for the dual polarised antenna sub-array

4. Summary

This benchmarking case has presented design and measurement data for 30 GHz single and dual polarised patch arrays fabricated using precision chemical etching on conventional Duroid substrates. The typical deviation of over 3% in the measured centre frequency from that predicted is high. It could be due to a combination of variations in material properties and fabrication dimensions. Based on the manufacturer's process specification, up to approximately 2% of the error (±35μm on each end of the 3 mm patch length) could be due to dimensional tolerance. The results highlight the need for accurate material and process characterisation, for example by means of sensitive resonator tests. In this case, a second iteration is called for, with the results of the first iteration fed back into the design algorithm. With such measures, and with systematic bias errors in dimensions and material properties separated from random errors, the upper frequency limit for patches produced by precision etching could be pushed considerably higher than the 30 GHz reported here.

The relatively high levels of cross polarisation radiation can be explained by the layout, and improved structures have been proposed.

European Commission - 6th Framework Programme	***ACE (Antenna Centre of Excellence)***	Information Society Technologies

Benchmarking Case on 63 GHz EDM Patch Antennas

Institution	**Authors**
Univ Birmingham	Ee LEE, Peter GARDNER, Peter HALL, Robert FOSTER

Document Evolution		
Revision	Date	Reason of change
0	28-11-05	

Benchmarking case on mm-wave Antenna Structures using Electric Discharge Machining (EDM)

1. Objective

The objective of this section is to describe the design and fabrication of air spaced mm-wave patch antennas fabricated using Electric Discharge Maching (EDM), in order to provide an example of the capabilities and limits of that technology.

2. Manufacturing Details

The structures described were designed to be manufactured by EDM, using a process available at the Department of Manufacturing and Mechanical Engineering at the University of Birmingham. The positional tolerance (i.e. how accurately the position of the centre of a line can be controlled) is +/- 0.1 microns. The typical tolerance in terms of the cut etc will be 5-10 microns. This can possibly be improved to a little better than 5 microns under "optimal" conditions, although such conditions are rare and ill defined.

3. Design and Simulation

Figure 1 shows a simple patch antenna design with a squarax transmission line and a squarax to waveguide transition. A simple supended line patch illustrated in Figure 1 has been simulated with a waveguide to sqaurax transition. This allowed a simple interface between the test setup and the antenna under test. Figure 2 shows the simulated return loss. Two resonant frequencies at 63 and 77 GHz were observed.

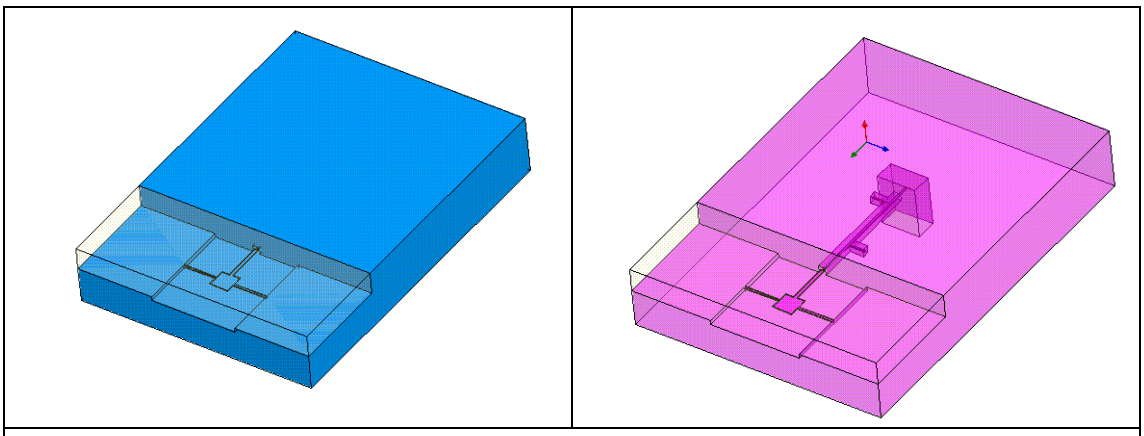

Figure 1

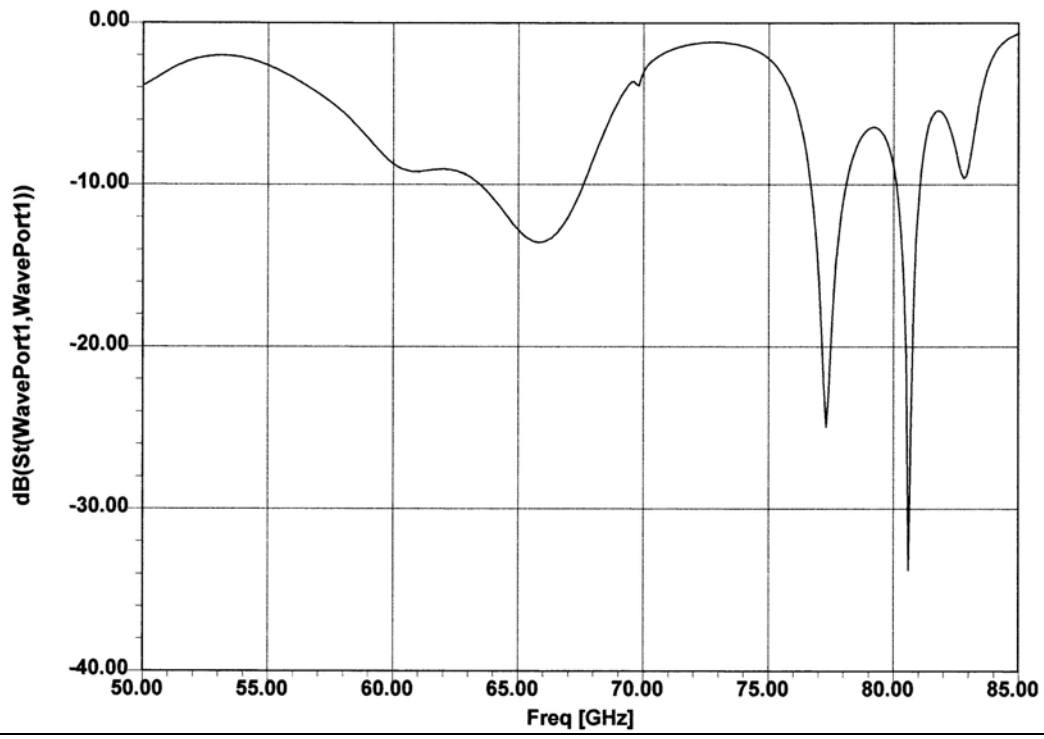

Figure 2

The design shown here has been manufactured using the EDM process within the University of Birmingham. Figure 3 shows a block machined to the required lateral dimensions. Figures 4 and 5 show high magnification views of details of the manufactured structures. The microscopy shows evidence of some over-etching slightly in excess of the process owners' estimates. The waveguide probe has a design width of 180 μm. Under the microscope, it was measured at 151.4 μm, suggesting over-etching by 14.3 μm on each side of the structure, as compared to the expected worst case of 10 μm. The next stage in the process, not yet completed, is to slice the block into layers of the appropriate thickness to form the centre conductor layer of the air spaced antenna and feed line. Further studies are ongoing to determine the applicability of the method for high frequency design.

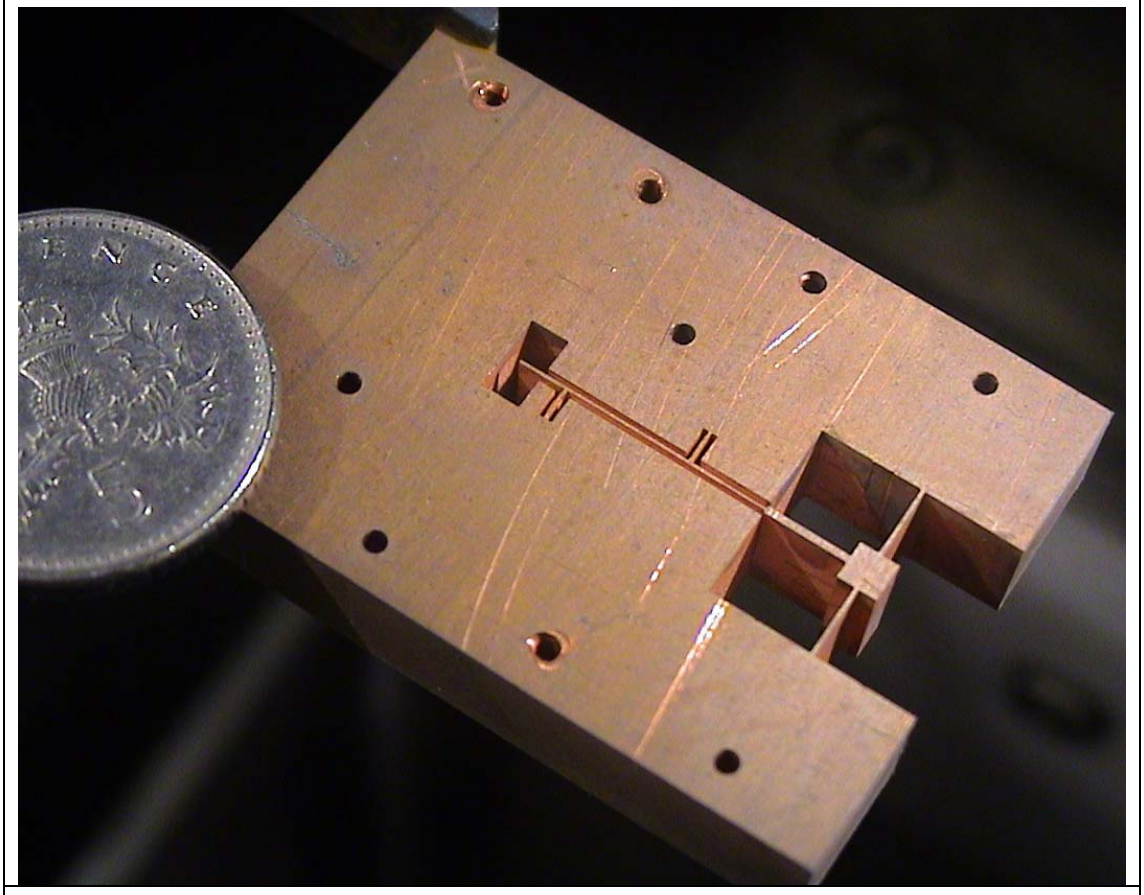

Figure 3

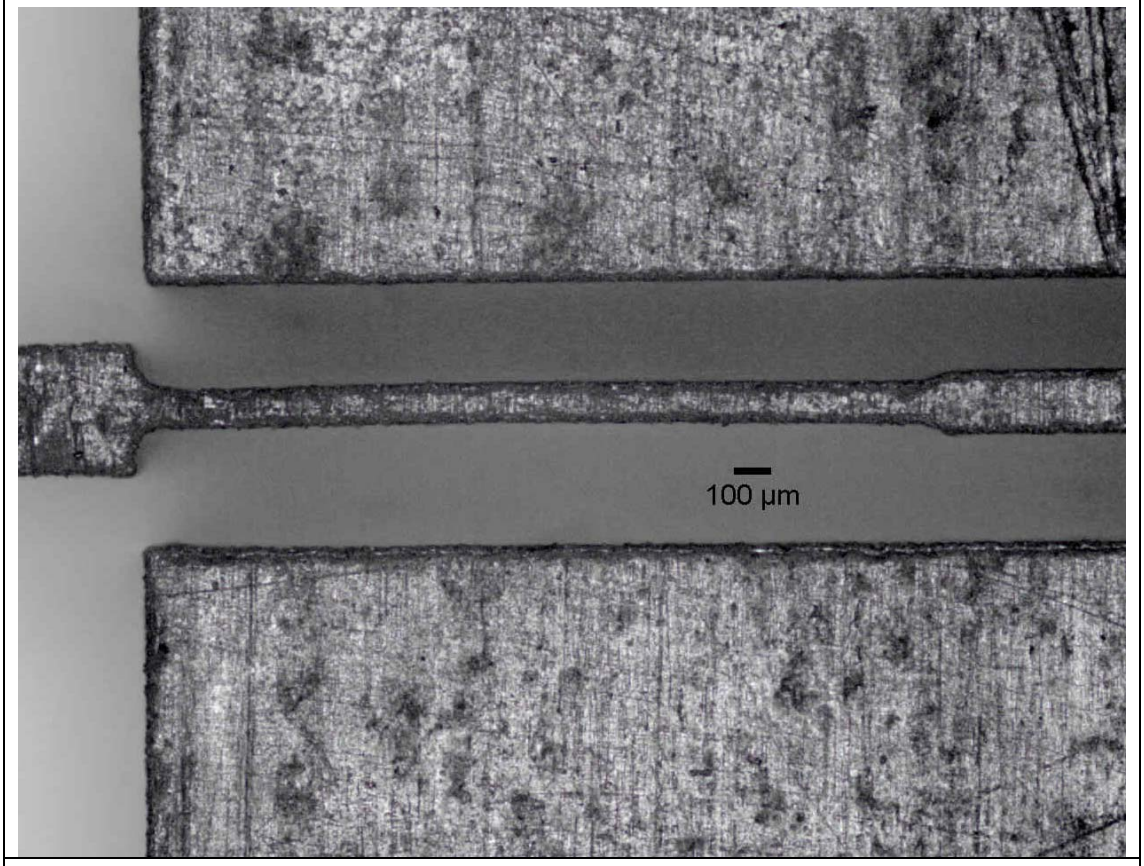

Figure 4

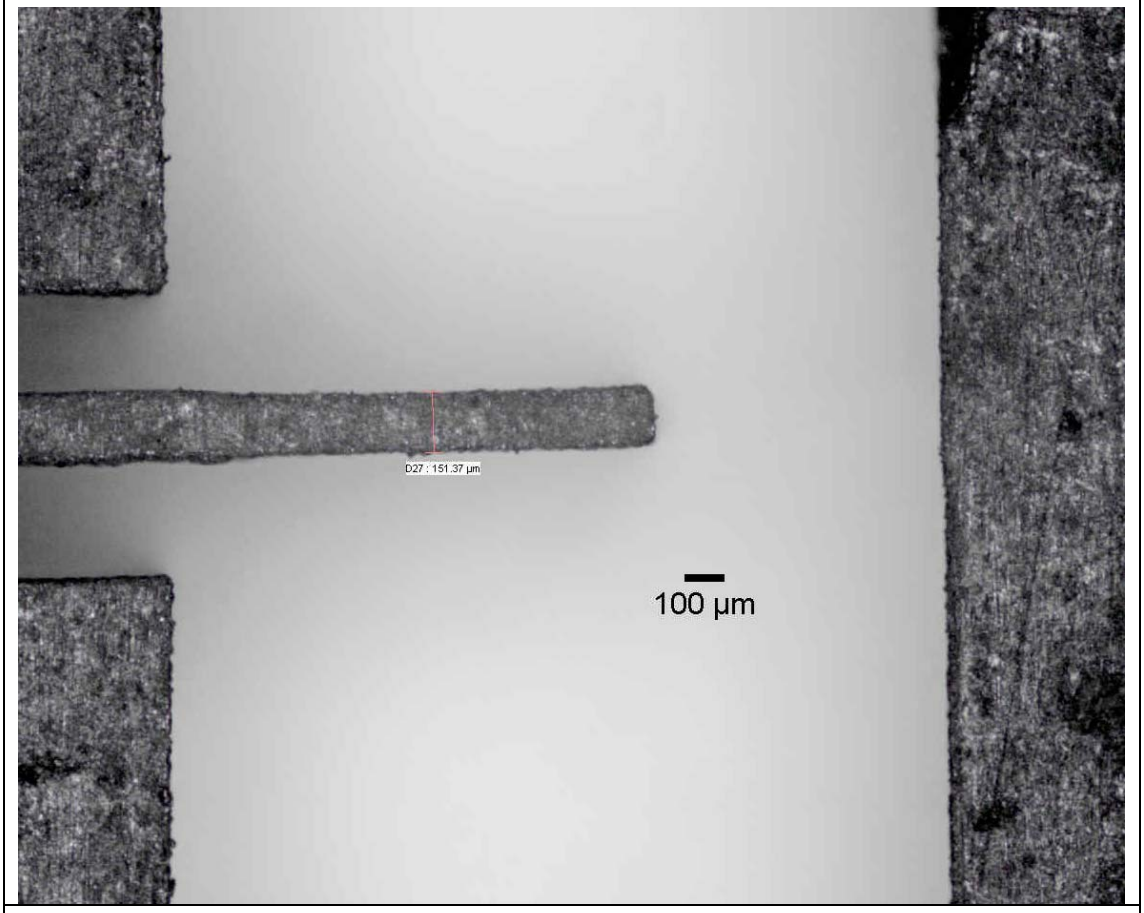

Figure 5

4. Summary and Conclusions

A process suitable for producing metalic structures with accurate lateral dimensions has ben demonstrated. Further work is required to generate thin layers suitable for air spaced squarax antennas and feedlines. Based on the typical dimensional tolerances of 10 microns, the accuracy of the resonant frequency of a 63 GHz half wavelength air spaced patch antenna (approximately 2.4 mm length) would be 0.26 GHz, or an error of 0.4%. The 14.3 μm error measured in practice would push this up to 0.37 GHz error, or 0.6%. It is likely that a more significant limitation would be in the tolerance of the input match to line impedance variations brought about by line width errors. Further work to analyse these is underway.

European Commission - 6th Framework Programme	***ACE (Antenna Centre of Excellence)***	Information Society Technologies

Benchmarking Case for Dielectric Rod Waveguide Antenna for 170 GHz

Institution	Authors
Helsinki University of Technology	Dmitri Lioubtchenko, Juha Ala-Laurinaho

Document Evolution		
Revision	Date	Reason of change
0	16.12.05	

1. OBJECTIVES

The objective of this section is to describe the design and fabrication of dielectric rod waveguide antennas for W and D bands.

2. INTRODUCTION

In this work antennas based on dielectric rod waveguide made of GaAs, fused sapphire and silicon cut along its optical axis inserted in the end of a standard metal waveguide is investigated with computer simulations and experiments in the W and D band. The radiation pattern is found to be similar to that of the open metal waveguide end, but less frequency-dependent beamwidth and input match: measured return loss is more than 25 dB.

The interest in design of high performance and low cost antennas in the millimeter wave band has increased in recent years due to developing millimetre-wave applications like high-speed wireless LANs, automobile collision avoidance radars, near-field probing in antenna measurements and also in applications using the frequencies approaching submillimetre-wave region. The dielectric rod waveguide (DRW) with a rectangular cross section combined with a metal waveguide is a promising candidate for these applications [1]. Dielectric rod waveguides made of materials with low dielectric permittivity (Teflon, polyethylene etc.) have been successfully employed as antennas [1-4]. The problem is, however, to provide a good matching of the DRW with a metal waveguide. Earlier it is shown that rectangular dielectric waveguides with high dielectric constant (>9) can be well matched with a standard metal waveguide by tapering the both feed and radiating ends of the rod to achieve losses less than 0.1 dB per transition [5, 6]. The dielectric rod waveguides were made of GaAs and monocrystalline Sapphire cut along its optical axis for W band and the dielectric rod waveguide for D band was made of silicon. Wide radiation patterns are possible due to a smaller size and a higher field concentration, in contrast to horn antennas or dielectric rod antennas made of low permittivity materials.

3. EXPERIMENTS

The experimental setups are shown in Figures 1 and 2. Dielectric rod waveguides were made of the GaAs (εr=13.3), monocrystalline Sapphire ($\varepsilon\perp$ = 11.56, $\varepsilon||$ = 9.39, $\tan\delta$ ~ 10-4) and silicon with resistivity of 5 kOhm/cm ($\varepsilon\perp$ = 11.9) cut along the optical axis. The designed transition, here to the WR-10 and WR-6 waveguides, does not require any horn structure that simplifies the construction. The rectangular cross section was chosen according to evaluations in [7] (k0b = 1.9, a/b = 0.5). Thus the dimensions ware 1.0x0.5 mm2 with 6 mm tapering section and 50-112 mm total lengths for W-band and 0.3x0.6 mm2 with 4 mm tapering section and 18 mm, 40 mm and 58 mm total length for D-band. The waveguide manufacturing was done in the Institute of Radioengineering and Electronics RAS, Moscow. The tolerances in manufacturing are described in [8].

The construction for W-band consists of a metal waveguide with a standard flange with pins, a Styrofoam holder and the tapered dielectric waveguide itself (Figure 1). Holes were drilled into the holder for the dielectric waveguide and two pins of the metal waveguide flange. Then the dielectric rod was inserted into the holder, and the holder was attached to the metal waveguide with the pins. The length of the tapering sections (6 mm) was chosen so that the tip angle was about 9° and the total length was 47 mm. The tapering is in the E-plane. The

ends of the Sapphire waveguide were tapered unsymmetrically for mechanical reasons, while for the GaAs waveguide they were tapered symmetrically. The construction for D-band antenna consists of a metal waveguide with a standard flange with pins and a Teflon holder (Figure 2). Tapering sections are 4 mm and the total length 58 mm.

Finite Element Method (FEM) with Agilent HFSS software was used to simulate, an ABmillimetre MVNA 8-350 was used to measure the radiation patterns of the antenna, and a HP 8510 VNA was used to measure the transmission loss and input return loss of the dielectric waveguides/antennas.

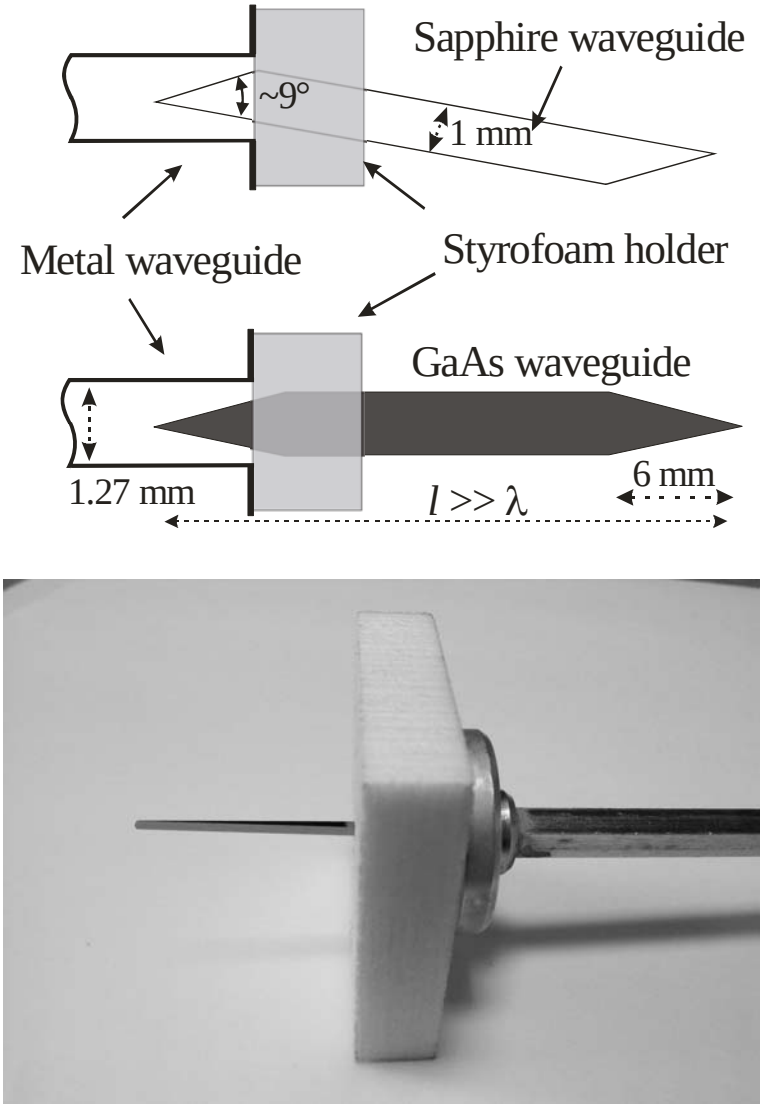

Figure1. Schematic structure and a photograph of the dielectric rod antenna with a transition to a WR-10 metal waveguide.

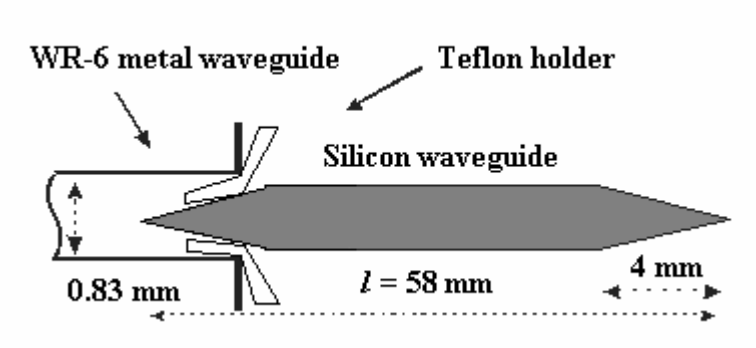

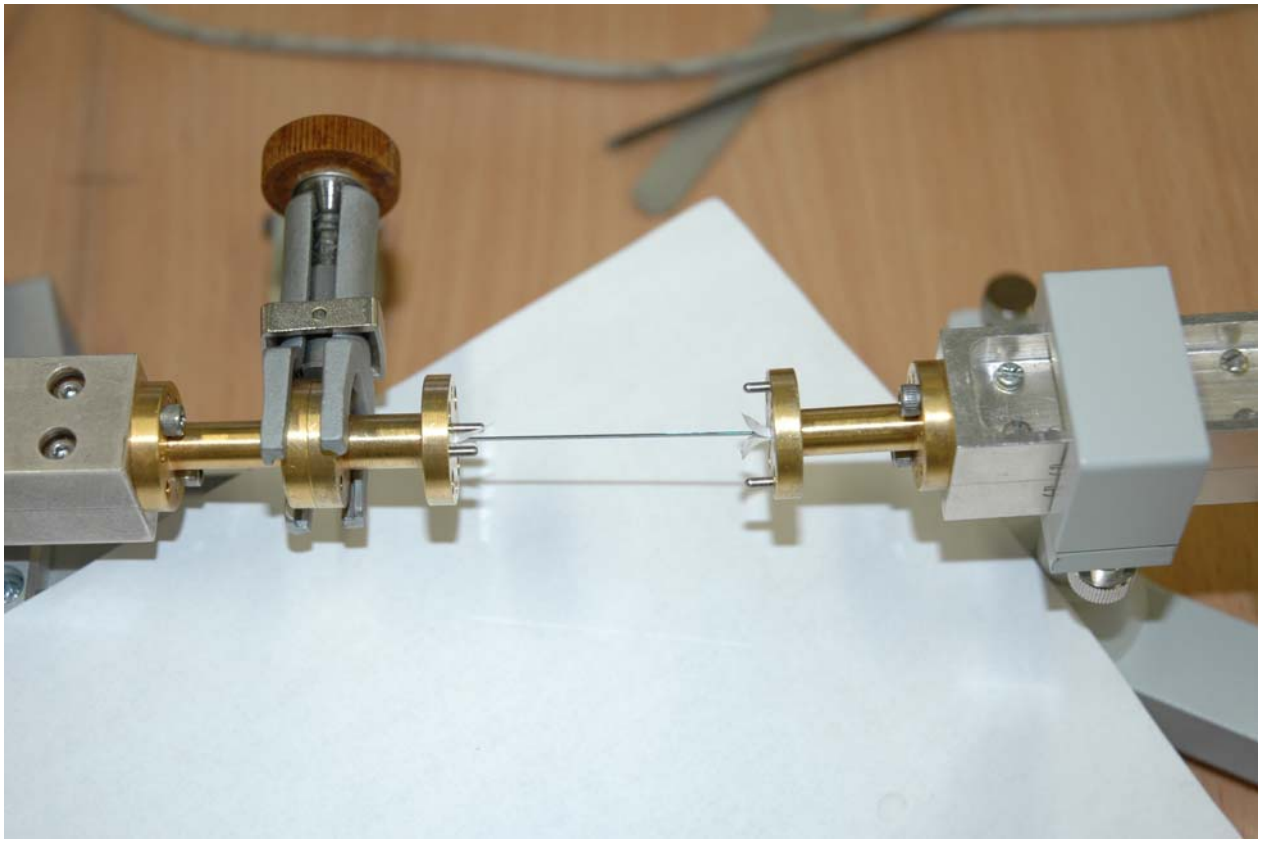

Figure 2. Schematic structure of the dielectric rod antenna with a transition to a WR-6 metal waveguide (above), Photograph of the measurement set-up for S-parameter measurements.

4. RESULTS

HFSS simulated radiation patterns of the W-band antennas are shown in Figure 3. The radiation patterns have quite wide beamwidth and there is a flat region around the boresight. The input return loss was also studied by simulation and found to be greater than 25 dB.

Before the DRW was used as an antenna, the S-parameters of the dielectric rod waveguides inserted between two metal waveguide ports were measured with a HP8510 VNA [5] (Figure4,5). The transmission loss was 0.05-0.35 dB for W-band and 0.5-1 dB for D-band. The return loss of the dielectric rod antennas was more than 25 dB both for the GaAs, Si and

Sapphire waveguide. In comparison, a WR-10 standard metal waveguide open end has a considerably lower return loss from 12 dB to 15 dB.

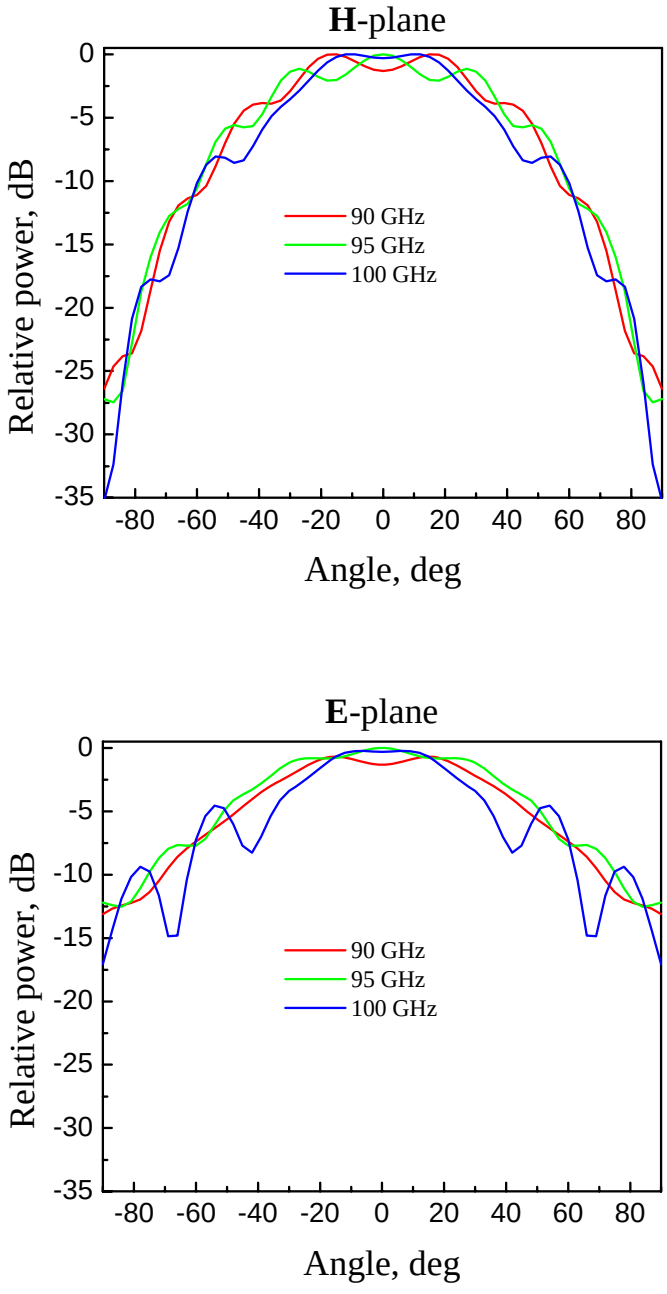

Figure 3. Simulated radiation pattern of the dielectric rod antenna made of Sapphire.

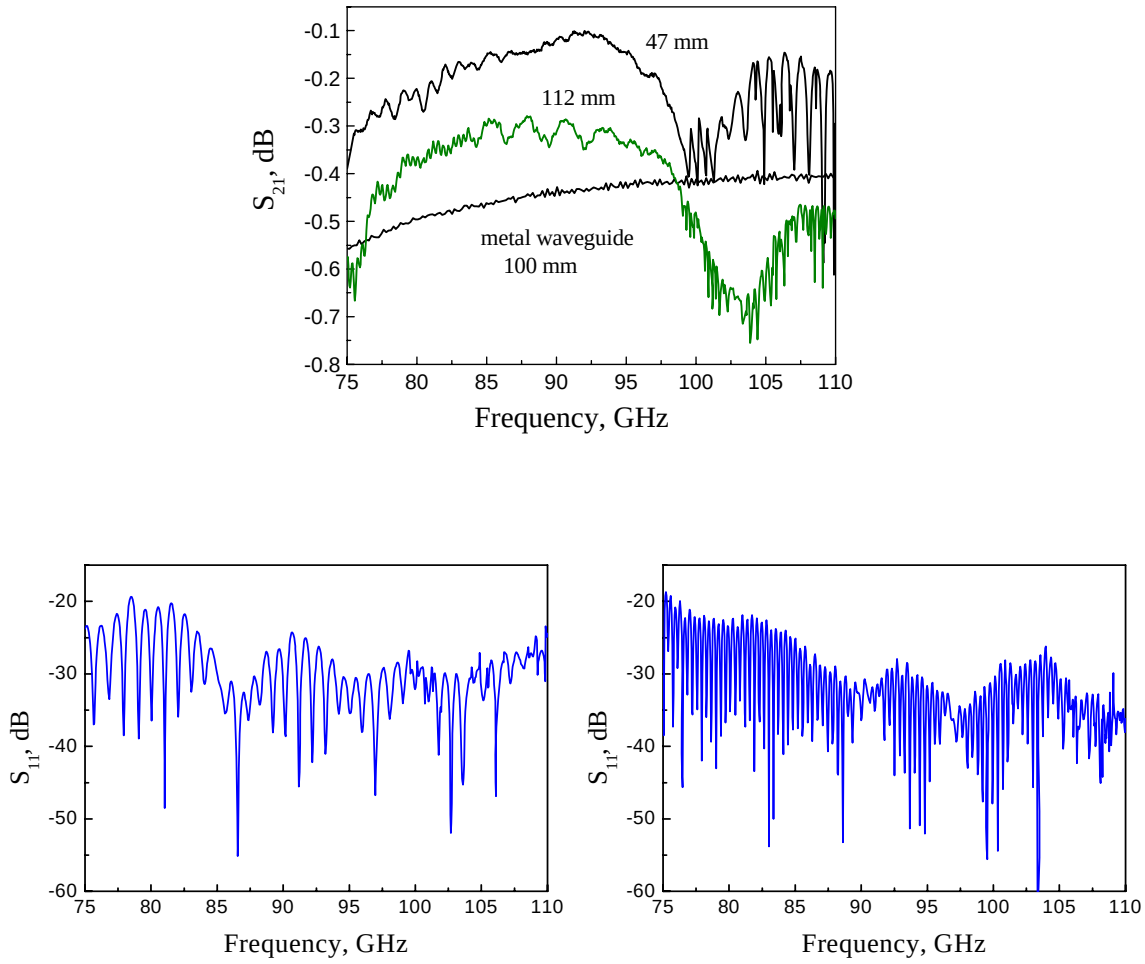

Figure 4. S-parameter measurements in W-band of sapphire DRW.

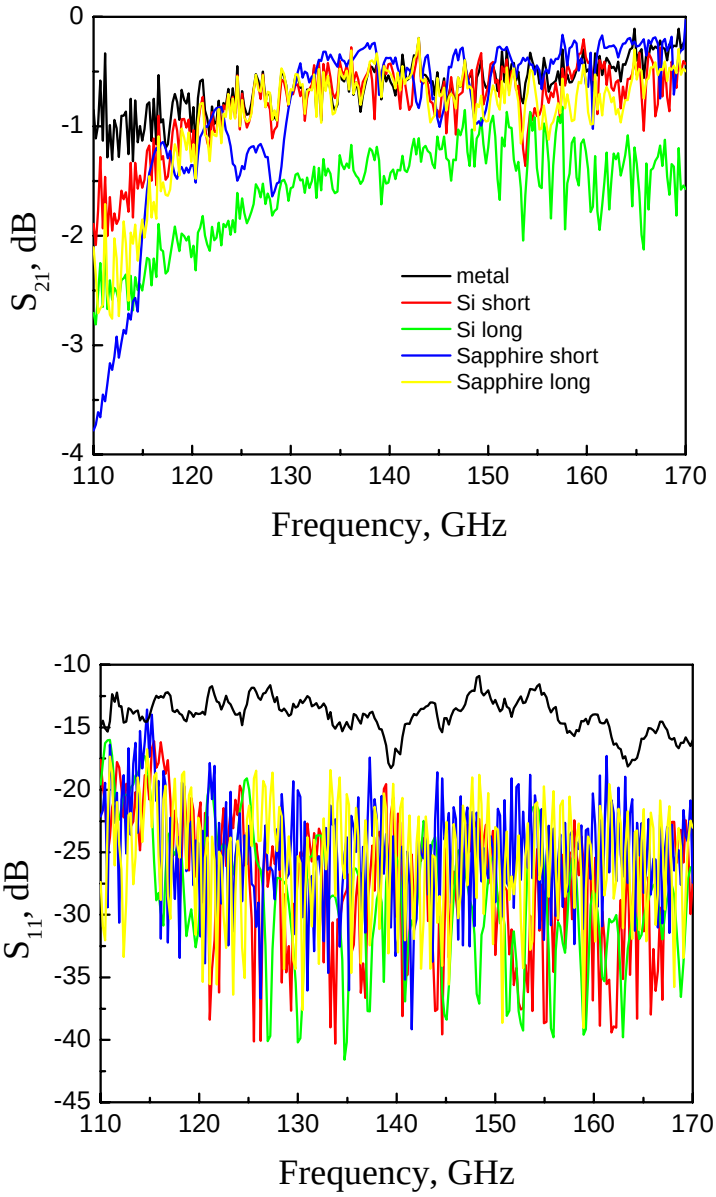

Figure 5. S-parameter measurements in D-band.

Radiation pattern measurements were carried out with an antenna rotator and the ABmillimetre MVNA 8-350 in both E- and H- planes. The results are shown in Figures 6 and 7 for W-band. The -3 dB beamwidths of the antennas are about 65-70 degrees in both E- and H-planes according to both measurements and simulations. The radiation patterns of the dielectric rod antennas are rather unchanged over the whole frequency band tested. In Figure 8, the radiation patterns of the D-band antenna are presented. The -3 dB beamwidths are about 50-60 degrees in both E- and H-planes. The radiation patterns are affected by poor dynamic range at the frequencies of 160 GHz and 170 GHz.

Appearance of small ripples in the radiation patterns, especially in the E-plane was observed both in simulations and experiments. Similar ripple characteristics have been observed

before by others [1, 2]. We believe that these ripples are related to an influence of the transition from the metal waveguide to the DRW, as most of the aperture area of the metal waveguide remains open. Note that in the experiments an absorber collar around the waveguide flange was used to suppress ripples observed in the radiation pattern.

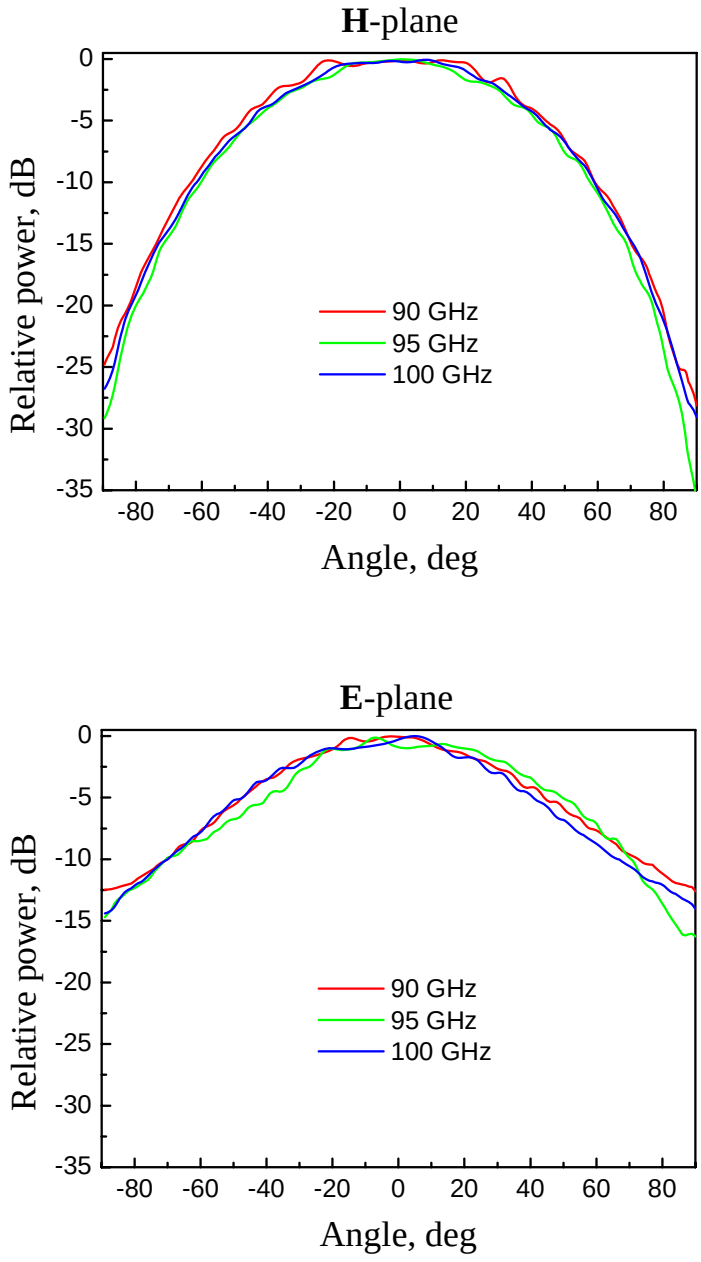

Figure 6. Measured radiation patterns of the Sapphire dielectric waveguide antenna.

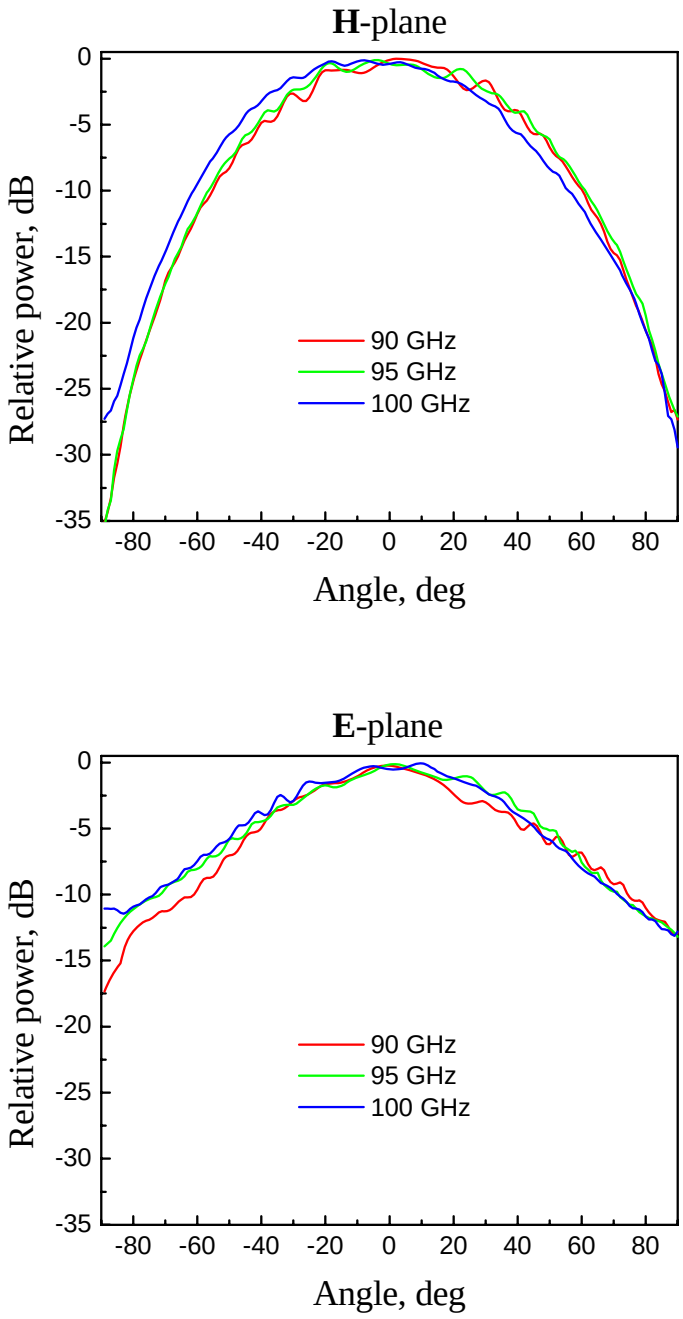

Figure 7. Measured radiation patterns of the GaAs dielectric rod waveguide antenna.

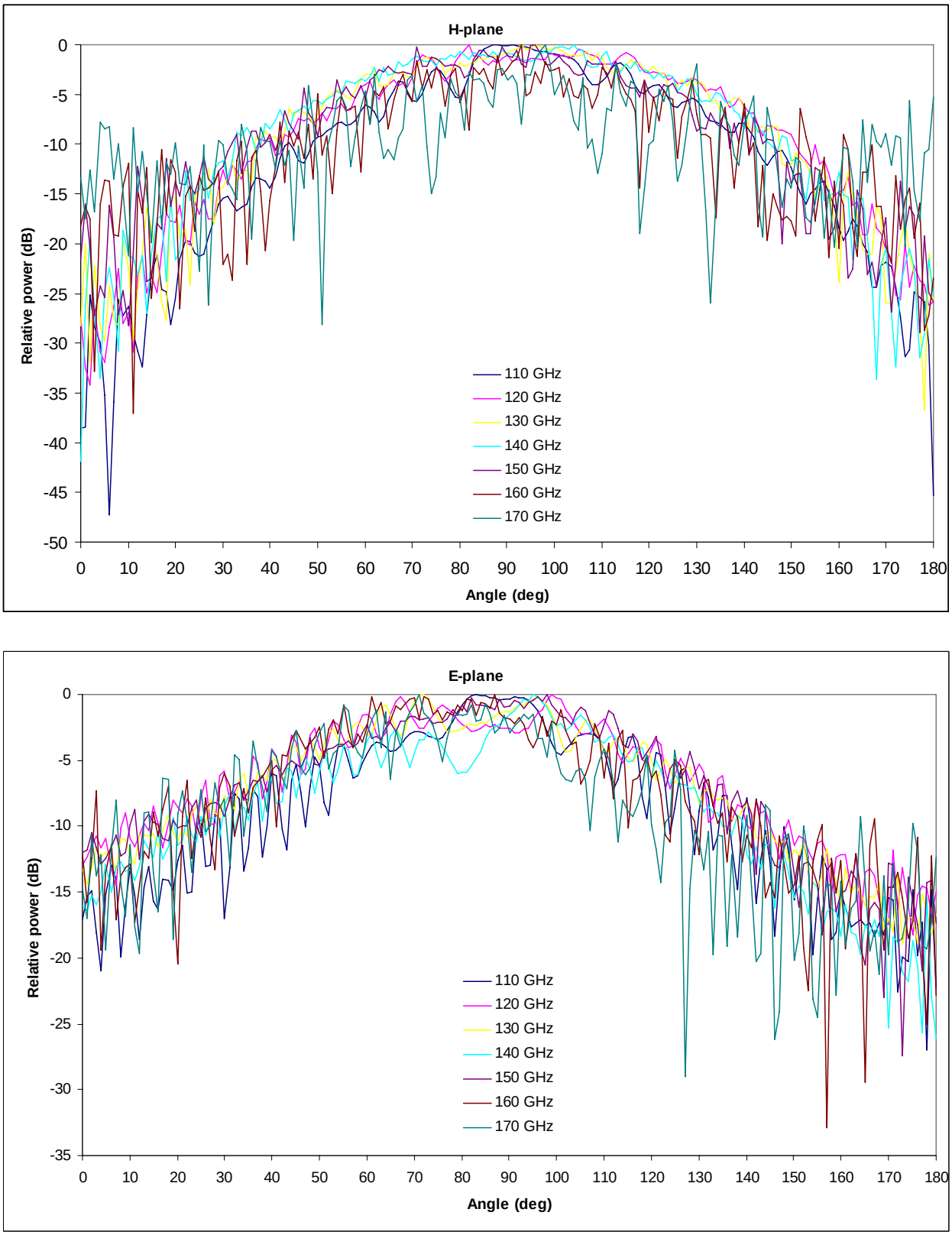

Figure 8. Measured radiation patterns of the silicon dielectric rod waveguide antenna for D band.

5. CONCLUSIONS

New dielectric rod antennas made of the GaAs, Si and Sapphire is proposed for the W and D-bands. These antennas possess a simple structure, light weight, and small dimensions, and they do not require a horn structure in the transition from the metal waveguide. The antennas offer broadband operation and high input return loss. Such antennas can be used as a feed of reflector type antennas, when a strong dependence of beamwidth on the frequency is undesirable, and could be attractive candidates for high-speed wireless LANs and near-field probing.

6. REFERENCES

[1] S. Kobayashi, R. Mittra, R. Lampe, “Dielectric rod antennas for millimeter-wave applications”, IEEE Trans. Antennas and Propagation, vol. AP-30, no 1, pp. 54-58, January 1982.

[2] Y. Shiau, “Dielectric rod antennas for millimeter-wave integrated circuits”, IEEE Trans. Microwave Theory and Tech., vol. MTT-24, no. 11, pp. 869-872, 1976.

[3] J. Weinzierl, Ch. Fluhrer, H. Brand, “Dielectric waveguides at submillimeter wavelengths” Proceedings of 6th International Conference on THz Electronics, 1998, U.K., pp. 166-169

[4] S.A. Yahaya, M. Yamamoto, K. Itoh and T. Nojima, “Dielectric rod antenna based on image NRD guide coupled to rectangular waveguide”, Electronics Letters, vol. 39, no. 15, pp. 1099-1101, 2003.

[5] D.V. Lioubtchenko, S. Dudorov, J. Mallat, J. Tuovinen, A.V. Räisänen, “Low loss sapphire waveguides for 75-110 GHz frequency range”, IEEE Microwave and Wireless Components Letters, vol. 11, no. 6, pp. 252-254, June 2001.

[6] D.V.Lioubchenko, S.N. Dudorov, A.V. Räisänen, “Development of rectangular open dielectric waveguide sections for the frequency range of 75-110 GHz”, Proc. of 31st European Microwave Conference, London, 2001, vol. 2, pp. 201-204.

[7] V.V. Meriakri, M.P. Parkhomenko, “Millimeter wave phase shifters based on ferrite dielectric waveguides“, 12th International Conference on Microwaves and Radar, MIKON 98, vol.2, 1998, pp. 514 -517.

[8] D. Lioubtchenko, S. Tretyakov, S. Dudorov, Millimeter-Wave Waveguides, KluwerAcademic Publishers, The Netherlands, 2003.